ANNUAL REVIEWS

Annual Review of Physiology

IP_3 Receptor Plasticity Underlying Diverse Functions

Kozo Hamada and Katsuhiko Mikoshiba

Laboratory of Cell Calcium Signaling, Shanghai Institute for Advanced Immunochemical Studies (SIAIS), ShanghaiTech University, Shanghai, 201210, China;
email: hamada@shanghaitech.edu.cn, mikosiba@shanghaitech.edu.cn

Annu. Rev. Physiol. 2020. 82:151–76

First published as a Review in Advance on November 15, 2019

The *Annual Review of Physiology* is online at physiol.annualreviews.org

https://doi.org/10.1146/annurev-physiol-021119-034433

Keywords

inositol 1,4,5-trisphosphate receptor, Ca^{2+} channel, gating mechanism, allosteric regulation, inositol 1,4,5-trisphosphate, endoplasmic reticulum

Abstract

In the body, extracellular stimuli produce inositol 1,4,5-trisphosphate (IP_3), an intracellular chemical signal that binds to the IP_3 receptor (IP_3R) to release calcium ions (Ca^{2+}) from the endoplasmic reticulum. In the past 40 years, the wide-ranging functions mediated by IP_3R and its genetic defects causing a variety of disorders have been unveiled. Recent cryo-electron microscopy and X-ray crystallography have resolved IP_3R structures and begun to integrate with concurrent functional studies, which can explicate IP_3-dependent opening of Ca^{2+}-conducting gates placed ~90 Å away from IP_3-binding sites and its regulation by Ca^{2+}. This review highlights recent research progress on the IP_3R structure and function. We also propose how protein plasticity within IP_3R, which involves allosteric gating and assembly transformations accompanied by rapid and chronic structural changes, would enable it to regulate diverse functions at cellular microdomains in pathophysiological states.

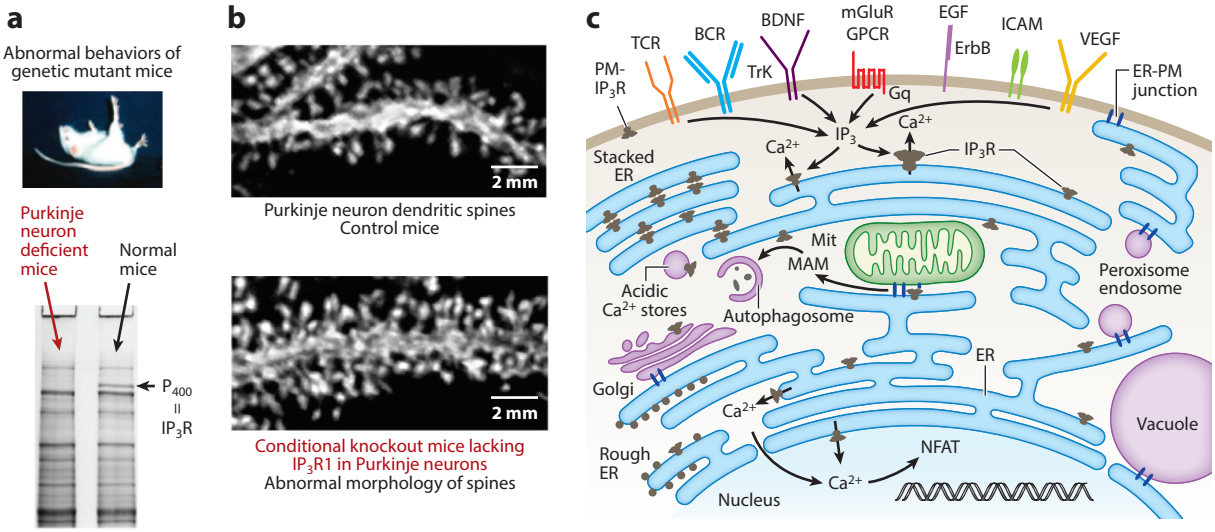

Figure 1

IP_3R functions at cellular microdomains. (*a*) In an early study of mutant mice showing motor defects, P_{400} proteins lacking in Purkinje neuron deficient mice were identified as the IP_3R (1, 184). Panel adapted with permission from Reference 184. Copyright 1985, S. Karger, AG. (*b*) Morphology of Purkinje neuron dendritic spines in control mice (*top*) and adult mice (*bottom*) lacking IP_3R1. Panel adapted from Reference 15 under the terms of the Creative Commons Attribution 4.0 International License, **http://creativecommons.org/licenses/by/4.0**. (*c*) IP_3 is liberated by G protein–coupled receptors (GPCRs), B cell receptors (BCRs), T cell receptors (TCRs), receptors for brain-derived neurotrophic factor (BDNF), vascular endothelial growth factor (VEGF), intercellular adhesion molecules (ICAMs), and epidermal growth factor (EGF) (185–188). IP_3 specifically binds to IP_3R and opens the Ca^{2+} channel. IP_3R-mediated Ca^{2+} release from Ca^{2+} stores, including the endoplasmic reticulum (ER) and acidic stores, should occur in various microdomains near the organelle, including mitochondria (Mit), plasma membrane (PM), Golgi, peroxisomes, endosomes, vacuoles, and autophagosomes. The ER contacts Mit at the mitochondria-associated membrane (MAM). Ca^{2+} activates gene expression via the nuclear factor of activated T cells (NFAT).

DISCOVERY OF P_{400}/IP_3R FROM THE BRAIN

In the 1970s, mutant mice with abnormal behaviors were studied, and a large membrane protein called P_{400}, which is highly abundant in cerebella of normal mice, was almost absent in Purkinje neurons of mutant mice showing motor defects (**Figure 1*a***) (1, 2). The mutant mice had poorly arborized dendrites in Purkinje neurons, while reduced P_{400} expression resulted in a loss of calcium ion (Ca^{2+}) spikes (3), suggesting a correlation of P_{400} with Ca^{2+} signaling. The P_{400} protein was purified (4) and its cDNA was isolated (5). Results showed that the P_{400} protein is an inositol 1,4,5-trisphosphate receptor (IP_3R) that releases Ca^{2+} from the endoplasmic reticulum (ER) in response to inositol 1,4,5-trisphosphate (IP_3) (6–8). Importantly, because the IP_3R channel cannot open without Ca^{2+}, the coincidence of IP_3 and Ca^{2+} is critical for channel activation (9, 10). To determine the physiological roles of IP_3R, knockout mice lacking IP_3R isoforms (IP_3R1, IP_3R2, or IP_3R3) were generated. Severe cerebellar ataxia (11), impaired long-term depression (12), and abnormal dendrites of Purkinje neurons (13) were found in mice lacking IP_3R1.

IP_3R: inositol 1,4,5-trisphosphate receptor

ER: endoplasmic reticulum

Recently generated knockout mice lacking IP_3R1 in the cerebellum and brainstem exhibited the same abnormal behaviors as the IP_3R1 knockout mice (14); however, conditional knockout mice specifically lacking IP_3R1 in Purkinje neurons showed only severe cerebellar ataxia (15). Interestingly, increased spine density and length (**Figure 1*b***) were observed even in adult mice, indicating the critical role of IP_3R1 in spine maintenance of Purkinje neurons in adults (15). The

IP_3R1-mediated regulation of spine morphology was elucidated by IP_3R-dependent activation of protein kinase C and consequent calmodulin (CaM)-dependent protein kinase IIβ (CaMKIIβ) phosphorylation, which modulates F-actin bundling to maintain spine structures (16). The gene expression of IP_3R is related to brain plasticity, and disrupted-in-schizophrenia 1, a susceptibility gene for major psychiatric disorders including schizophrenia, regulates the transport of mRNA encoding IP_3R1 for synaptic plasticity (17).

In addition to IP_3R1, knockout mice lacking IP_3R2 showed impairments of astrocytic Ca^{2+} surge and neuronal plasticity by transcranial direct current stimulation, which enhances memory and cognition in humans (18). A number of prominent studies indicate that IP_3R2 was the major isoform in astrocytes because a large part of calcium signaling is attenuated in IP_3R2 knockout mice (19, 20). However, this has been debunked by recent studies. Ca^{2+} imaging of hippocampal slices revealed that IP_3R2 and IP_3R3 were functional in astrocytes and also suggested the presence of functional IP_3R1 in astrocytes (21). A study using a highly sensitive Ca^{2+} indicator clarified Ca^{2+} release in cortical and hippocampal astrocytes of IP_3R2 knockout mice (22). These data shed light not only on IP_3R2 but also IP_3R1 and IP_3R3 that are involved in astrocytic functions.

In the past 40 years, numerous studies have clarified the diverse functions of IP_3R in living systems, ranging from unicellular organisms to our bodily organs, including the brain; however, how to achieve these diverse functions remains a mystery. Here, we review recent advances in researching the cellular microdomains and protein structures of IP_3R and discuss how to approach a possible linkage between the diverse functions of IP_3R and their structural dynamics that we refer to as IP_3R plasticity.

PM: plasma membrane

MAM: mitochondria-associated membrane

IRBIT: IP_3R-binding protein released with IP_3

DIVERSE FUNCTIONS OF IP_3R AT MICRODOMAINS

IP_3R is abundant in the smooth ER and is localized at lower levels in rough ER (23), the Golgi (24), the nucleus (25–27), and the plasma membrane (PM) (28, 29) (**Figure 1*c***). Nuclear IP_3R plays an important role in gene transcription (30, 31) and is expressed in nuclear calcium stores to mediate nuclear signaling and cause nuclear translocation of protein kinase C (30, 31). Apoptosis induces mixed clusters of IP_3R1 in the nucleus (32), and IP_3R1 gene expression in hippocampal CA1 is decreased by neonatal anoxia, which triggers translocation of IP_3R1 to the nucleus and neuronal cell death (33). In addition to the nucleus, reports show that IP_3R can locate at the PM of neurons (28), lymphocytes (34), platelets (35), and hepatocytes (36). The studies using chicken B cells lacking endogenous IP_3R have clarified Ca^{2+} influxes via a limited population of the PM-IP_3R (37, 38). IP_3R is also located within acid Ca^{2+} stores (39–41), which can control autophagy in *Trypanosoma brucei* (42).

The IP_3R protein also operates at membrane contact sites between the ER and other organelles (**Figure 1*c***). For example, membrane contact sites between the ER and mitochondria, so called mitochondria-associated membranes (MAMs), facilitate transport of Ca^{2+} from the ER to mitochondria (43, 44). The voltage-dependent anion channel on the outer mitochondrial membrane binds to the IP_3R via the molecular chaperone glucose-regulated protein 75, and the protein complex links the ER to mitochondria and facilitates Ca^{2+} transport (45). The mammalian TOR complex 2 interacts with the complex at the MAM (46), and it is proposed that autophagosomes could be formed at the MAM (47, 48). An interaction between the ER protein Bap31 and the mitochondrial fission protein Fission 1 homolog should regulate the induction of apoptosis (49). Ca^{2+} transport at the MAM has Janus-faced roles and cancer cells require IP_3R-mediated Ca^{2+} transfer from the ER to mitochondria for survival, while normal cells induce autophagy for survival by impaired Ca^{2+} transfer (50). The IP_3R-binding protein released with IP_3 (IRBIT) is involved in MAM function and structure because the IRBIT knockout reduced staurosporine-induced

EM: electron microscopy

IBC: IP_3-binding core

SD: suppressor domain

apoptosis and mitochondrial Ca^{2+}. In particular, the phosphorylated form of IRBIT (P-IRBIT) likely regulates MAM structure and function (51). IP_3R also associates with the sigma-1 receptor (Sig-1R), an integral ER membrane protein that regulates IP_3R at the MAM (52). Recently, choline produced by phospholipase D was found to be an endogenous agonist of Sig-1R to potentiate Ca^{2+} signals evoked by IP_3R as an intracellular messenger (53).

The ER frequently contacts the PM in neurons (54, 55) and non-neuronal cells (56, 57). Electron cryotomography (cryo-ET) imaging revealed that the ER-PM contact is mediated by extended synaptotagmins in addition to stromal interaction molecule 1 (55). The ER-PM contact is also mediated by ER-resident Sec22 and PM syntaxins (54). The ER forms ER-PM junctions in pancreatic acinar cells (56), and IP_3R-containing ER-PM junctions accumulate at the leading edge of focal adhesions during cell migration (57). In fibroblasts, interleukin (IL)-1 promoted colocalization of protein tyrosine phosphatase α (PTPα) and focal adhesion kinase (FAK) with the ER and increased association of IP_3R1 with PTPα and FAK at focal adhesions near the PM (58).

In the brain, ER-ER contacts are frequently observed in the cell body and dendrites of Purkinje neurons, and electron microscopy (EM) clarified that the stacked ER is enriched with IP_3R (23, 59–61). In the stacked ER, two apposed IP_3Rs bridge between ER layers (61), and this finding is supported by formation of a stacked ER in cells upon overexpression of full-length IP_3R but not by deletion mutants (62). The brief anoxia of oxygen-deprivation (3 min) is enough to cause formation of a stacked ER in Purkinje neurons (63), which is reversible by reoxygenation (64). While structural data has accumulated, physiological roles of the stacked ER remain unknown. A putative Bcl-2 inhibitor apogossypol induced ER aggregation, caused by reorganization of the ER membrane in various cell lines and even in the fission yeast (65). Apogossypol-stimulated Ca^{2+} efflux from the ER is partially mediated by IP_3R because 2-aminoethoxydiphenyl borate, an inhibitor of IP_3R and the transient receptor potential (TRP) channel, completely blocked the apogossypol-dependent ER aggregation (66), but the mechanism is not clear. Membrane contact sites between the lysosomes and the ER/sarcoplasmic reticulum would regulate Ca^{2+} release by lysosomes, but the mechanism is not clearly understood (67). The ER also makes contacts with the other organelles such as phagosomes, peroxisomes, endosomes, and vacuoles (68, 69), but the functional roles of the IP_3R in these contact sites remain unknown.

IP_3R STRUCTURE AND FUNCTIONAL DOMAINS

The genes for three IP_3R subtypes (IP_3R1–3) were cloned from various vertebrates (5, 70–73). All vertebrate IP_3R genes encode a large cytosolic domain and a small Ca^{2+} channel domain (**Figure 2*a***). Approximately 55% of amino acid residues in the full-length mouse IP_3R1 are conserved among the three isoforms, particularly in the critical regions responsible for IP_3R function. Molecular cloning uncovered alternative splicing sites (SI–SIII) (**Figure 2*a***) in rodents (73–75) and humans (76), giving rise to phenotypic diversity of IP_3R channels, and RNA processing at these splicing sites is controlled during development and differentiation (74, 75, 77).

The cytosolic domain contains key functional domains, including an IP_3-binding core (IBC) (78), an adjacent amino (N)-terminal suppressor domain (SD) that reduces the affinity of IP_3 binding (79), and large regulatory/coupling domains containing various allosteric sites for phosphorylation, binding proteins, and regulators including Ca^{2+} (**Figure 2*a***). IBC is the minimum region required for specific IP_3 binding and is mapped within residues 226–578 of mouse type-1 IP_3R (IP_3R1). The crystal structure of IBC (residues 224–604) in a complex with IP_3 was determined at a resolution of 2.2 Å (80). Early electron microscopy (EM) studies predicted that the IBC could be located at the top surface distant from the channel domain (81, 82). The most recent cryo-EM studies clarified the precise location of IBC (**Figure 2*b***) (83–85). Eleven amino

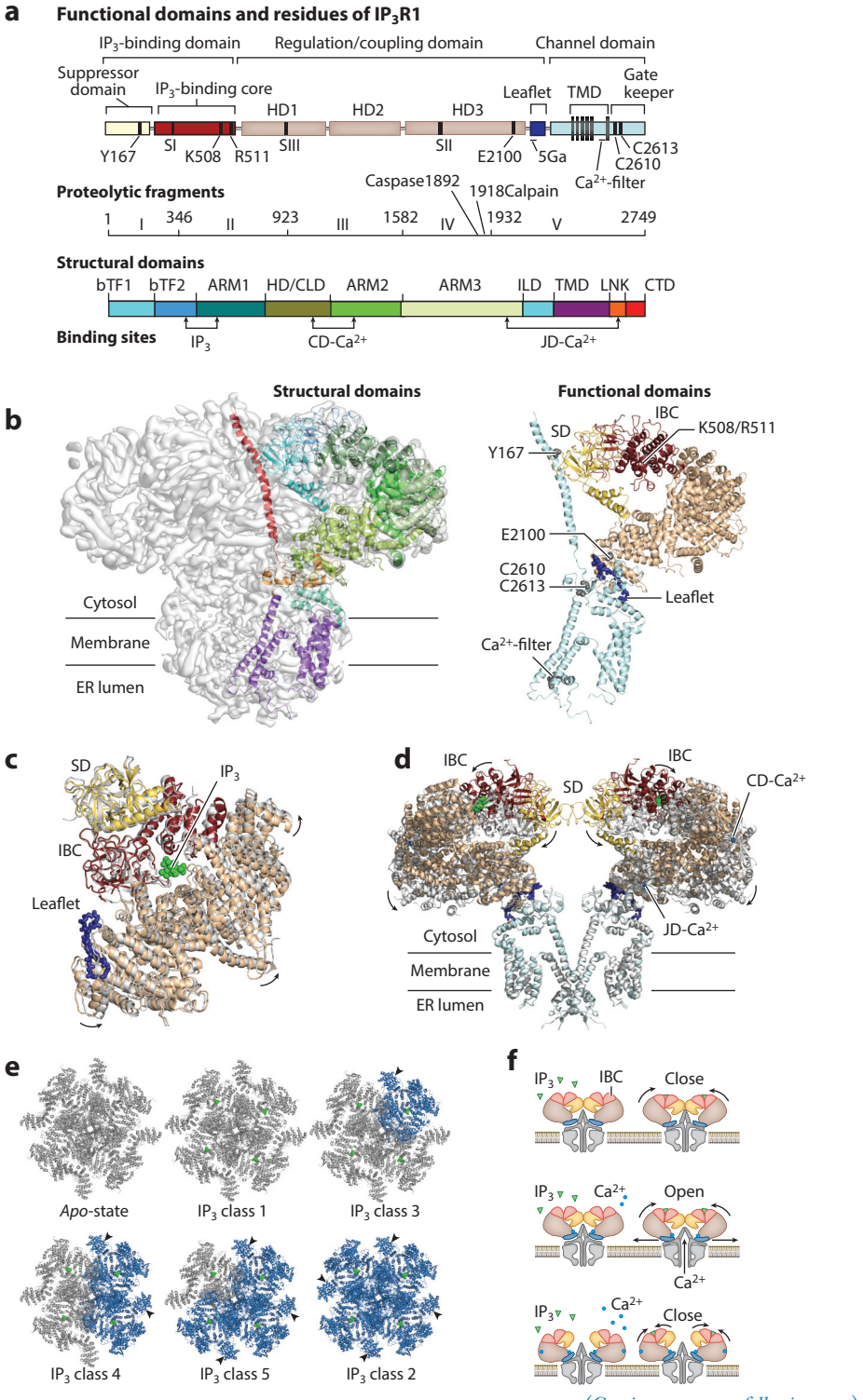

(*Caption appears on following page*)

Figure 2 (*Figure appears on preceding page*)

IP_3R structures and allosteric gating. (*a*) Schematic primary structures of IP_3R. The upper panel shows functional domains and critical residues in IP_3R1 (78, 79, 116), and proteolytic fragments of IP_3R1 are drawn below (6). Each domain is depicted in a different color: suppressor domain (SD) in yellow (amino acid residues 1–225); IP_3-binding core (IBC) in red (residues 226–604); the large regulation/coupling domain in tan, including α-helical domain 1 (HD1; residues 605–1,009), α-helical domain 2 (HD2; residues 1,026–1,493), α-helical domain 3 (HD3; residues 1,593–2,217), and channel domain in pale blue (residues 2,218–2,749). The bottom panel shows structural domains of IP_3R (84), and IP_3/Ca^{2+}-binding sites are indicated by arrows. Alternative splicing sites are indicated by SI, SII, and SIII. (*b*) The 3D structure of IP_3R1. The left panel shows a cryo-EM map (EMD9244) with a model (6MU2) of structural domains. The right model delineates functional domains and critical residues. (*c*) Conformational changes induced by IP_3. Comparison of an X-ray crystal structure resolved in the absence (*colored*) or presence (*gray*) of IP_3. Two X-ray crystal structures of IP_3R2217 were superimposed by fitting the N-terminal β-rich domain (residues 7–430) (112). (*d*) Ca^{2+}-dependent conformational changes demonstrated by IP_3-bound and IP_3/Ca^{2+}-bound cryo-EM structures of hIP_3R3 (85). (*e*) Conformational ensemble in IP_3-bound states. Structures of *Apo*-state, IP_3 class 1, IP_3 class 3, IP_3 class 4, IP_3 class 5, and IP_3 class 2. The relocated HD2/ARM2 domain of each subunit (*blue*) is indicated by an arrow (85). (*f*) Allosteric gating and its regulation. Schematic model in the absence of Ca^{2+} in which IP_3 can bind, resulting in an ensemble of distinct conformations, but it cannot open the channel gate (*top*). In contrast, IP_3 can open the channel gate in the presence of low Ca^{2+} that can bind to a Ca^{2+} sensor, probably the JD-Ca^{2+} site near E2100 and the leaflet (*middle*). In case of high Ca^{2+}, IP_3 cannot open the channel gate because Ca^{2+} binds to the inhibitory Ca^{2+} site, presumably the CD-Ca^{2+} site, which could induce large conformational changes and subunit dissociations (*bottom*).

acid residues, including K508/R511 in the IBC domain, are responsible for the correct recognition of IP_3; all of these residues except Gly268 are conserved in the other IP_3R isoforms (72, 86). Molecular dynamics simulation of IBC suggests that the conserved Arg241-Glu439 salt bridge determines flexibility of the IBC domain in the ligand-free state (87).

The SD functions as a suppressor for IP_3 binding, and the deletion of SD results in a significant enhancement of IP_3 binding (78, 79). The atomic resolution structure of the SD of mouse IP_3R1 was determined using X-ray crystallography at a resolution of 1.8 Å (88). The location of the SD was unexpectedly different from some predictions of the direct coupling of the SD to the channel domain (**Figure 2*b***). Mutagenesis indicated that the residue Y167/W168 in the SD is critical for IP_3-induced Ca^{2+} release, but not for IP_3-binding (89). Thus, the Y167/W168-containing hot-spot loop (HS-loop) was proposed to be located near the channel. However, all structures determined by recent cryo-EM studies have demonstrated that the HS-loop is far from the channel domain and is located close to the interfaces between subunits (**Figure 2*b***). Therefore, the HS-loop should be considered necessary for subunit interaction rather than direct coupling to the channel.

Because the SD inhibits IP_3 binding within the IBC domain, the SD was considered to bind and mask the IP_3-binding pocket directly. The N-terminal 604 residues containing the SD and IBC domain showed ∼50 nM of dissociation constant for IP_3 (IP_3R1), ∼14 nM for IP_3R2, and ∼160 nM for IP_3R3 (90). These values are close to those of the full-length IP_3Rs (73), whereas the IBCs of all subtypes show identical affinities (∼2 nM) for IP_3, suggesting that the subtype-specific IP_3-binding affinities should be due to each SD. Analyses of site-directed mutagenesis on the SD of mouse IP_3R1 showed that seven conserved amino acid residues are critical for the suppression of IP_3 binding (88) and that eleven IP_3R3 specific loops were critical for the IP_3R3-specific IP_3-binding affinity (90). Therefore, direct association of these residues to the IP_3-binding pocket was proposed. The first X-ray crystal structures (3.8 Å) showing IP_3-dependent conformational changes were solved using the N-terminal domain of rat IP_3R1 (residues 7–602 and 322–336 were removed) and then recombinant protein (residues 1–604) with mutated cysteine residues. In both X-ray crystal structures, unexpectedly the SD did not mask the IP_3-binding pocket itself (91, 92),

suggesting that these critical residues for suppression of IP_3 binding may fix IBC conformation. All-atom molecular dynamics simulations of the N-terminal domains, including the SD and IBC, demonstrated the characteristic twist motion of the SD and revealed the correlated dynamics of IBC with IP_3 binding (93). These reports could elucidate the mechanism of how the SD affects the conformational changes of IBC. However, the role of the HS-loop, including Y167/W168, still remains unknown. Ca^{2+} imaging using IP_3R-null HeLa cells generated by genome editing revealed that mutations in a genetic brain disorder, spinocerebellar ataxia 29 (SCA29), identified within or near the IBC completely abolished channel activity (94). Interestingly, a major part of these mutations showed impaired IP_3 binding to IP_3R1, whereas the T579I and N587D mutations disrupted channel activity without affecting IP_3 binding, suggesting that these two residues should be involved in allosteric regulation.

SCA: spinocerebellar ataxia

RyR: ryanodine receptor

Although Bikonta IP_3R does not have completely conserved critical residues in the IP_3-binding site, and the endogenous IP_3R of *Trypanosoma cruzi* is localized in acid Ca^{2+} stores but not in the ER (40), they exhibit IP_3-binding activity in *Paramecium* (95) and *T. cruzi* (96). The IP_3-evoked Ca^{2+} release activities in *Paramecium* tetraurelia (95), *T. brucei* (41), and *T. cruzi* (96) have been confirmed. *T. cruzi* is the pathogenic parasite of Chagas disease, whereas *T. brucei* causes African trypanosomiasis or sleeping sickness. Therefore, they should be drug targets because IP_3R controls cell death events in parasites (97).

CONFORMATIONAL CHANGES IN IP_3R

To date, the basic mechanism by which local conformational changes in the IBC can open the Ca^{2+} channel in the IP_3R remains elusive because of difficulties associated with studying allosteric mechanisms over the long distance between IP_3-binding sites and the Ca^{2+} channel. Among the known ligand-gated ion channels whose atomic structures have been solved by X-ray crystallography or cryo-EM, such as the nicotinic acetylcholine receptor (98), NMDA (99), AMPA (100), $GABA_A$ (101), 5-HT_3 (102), P_2X (103), and ryanodine receptor (RyR) (104), the distance from ligand-binding sites to the Ca^{2+} channel in IP_3R is the longest.

Early EM studies on tetrameric IP_3R structure were performed by negative staining of purified IP_3R (81, 105–107), and cryo-EM studies were published from several groups (82, 108, 109); however, their published maps showed different structures, and the discrepancies have been discussed in review papers (110, 111). Thereafter, the IP_3 receptor structure at a 17-Å resolution was published, followed by the recent revolution of cryo-EM technology that uncovered the structure of IP_3R at a 3- to 5-Å resolution (83–85). These high-resolution maps of IP_3R show the mushroom-shaped structure consistent with early negative-stained images (81), whereas the cryo-EM structure in the presence of Ca^{2+} shows an opened structure with disrupted subunit interactions (85), which is in line with the early negative staining studies (81, 106).

Recently, crystallization of a truncated IP_3R1 including 2,217 residues (IP_3R2217) was reported (112). Rod-shaped diffracting crystals of IP_3R2217 and the bipyramidal crystals of a truncated IP_3R1 including 1,585 residues (IP_3R1585) were obtained, and X-ray crystal structures of the mouse IP_3R1 cytosolic domain were determined at a resolution of 5.8 to 7.4 Å. The crystal structure of the large cytosolic domain of IP_3R2217 could assign five domains: an N-terminal SD, IBC, and three curvature helical domains (HD1–3) (**Figure 2*c***). Comparison of IP_3R2217 structures in the absence and presence of IP_3 shows conformational changes by IP_3 (112).

Among the various regulators, which modulate IP_3-dependent channel opening by binding to discrete allosteric sites, Ca^{2+} is the most important regulator for IP_3R (6, 9, 10). In 2002, the first article about Ca^{2+}-induced global structural changes in tetrameric IP_3R1, revealed by negative-staining EM and limited enzymatic proteolysis, was published (106). The results were confirmed

JD-Ca^{2+}: juxtamembrane domain Ca^{2+}

CD-Ca^{2+}: cytoplasmic domain Ca^{2+}

by Ca^{2+}-dependent accessibility with large polyethylene glycol maleimide molecules (113). This finding was confirmed in living cells using fluorescence resonance energy transfer between two fluorescent proteins fused to the N terminus of individual subunits (114). Ca^{2+} rigorously determines the channel activity of IP_3R and a low Ca^{2+} level acts as an essential coagonist for IP_3-gated Ca^{2+} release, whereas a high Ca^{2+} level inversely acts as a feedback inhibitor (9, 10). This bell-shaped regulation suggests the existence of an activation site and an inhibitory site for Ca^{2+} binding in the IP_3R. Early biochemical analyses using Ca^{2+} overlay suggest various Ca^{2+}-binding sites (115). Accordingly, Ca^{2+}-binding sites should be distributed not only in the IBC/SD or channel domains but also in the large regulatory/coupling domains. A recent cryo-EM study uncovered the molecular detail upon the global conformational changes in the tetrameric human IP_3R3 (**Figure 2*d***) (85). Notably, the cytosolic domain of hIP_3R3 solved by cryo-EM in the presence of high Ca^{2+} concentrations is almost consistent with the X-ray crystal structure of mIP_3R1 (112). The cryo-EM structures in the presence of Ca^{2+} reveal two Ca^{2+}-binding sites in the regulatory/coupling domains, and a high concentration of Ca^{2+} induces the disruption of numerous interactions between subunits, which confirmed the earlier studies and clarified the Ca^{2+}-dependent inhibition mechanism at a high resolution (85). The juxtamembrane domain (JD)-Ca^{2+}, near the residue corresponding to E2100 of IP_3R1 (116), should be presumably critical for Ca^{2+}-dependent activation. By contrast, the cytoplasmic domain (CD)-Ca^{2+}-binding site is located between two structural domains, an armadillo-repeat domain 2 (ARM2) and a central linker domain, suggesting that CD-Ca^{2+} should stabilize the spatial relationship between these domains and that this conformational change should be a causal factor for subunit interaction. The large structural change by dissociation between subunits has never been reported in RyR, even though RyR is regulated by Ca^{2+} in a bell-shaped manner similar to IP_3R. This difference could be due to the distinct property between RyR and IP_3R, and we could speculate that the intersubunit interaction in the IP_3R tetramer should be weaker than that in RyR. The large-scale structural change by Ca^{2+} could elucidate the inhibitory mechanism of high Ca^{2+} concentration, but how the low concentration of Ca^{2+} could induce conformational changes to activate the IP_3-dependent channel gating remains unclear.

A recent study about IP_3R in unicellular organisms demonstrated the important features of Ca^{2+}-dependent regulation. Many putative IP_3R genes in unicellular organisms encode the conserved amino acid sequence at the pore, and critical amino acid residues within IP_3-binding sites are also conserved in Holozoa, including *Capsaspora*, but not in fungi and earlier organisms. The most recent study of IP_3R in *Capsaspora owczarzaki* demonstrated that IP_3R targets the ER, binds IP_3, exhibits Ca^{2+} release activity, and forms hetero-oligomers (117). Therefore, the *C. owczarzaki* gene should be a common ancestor of vertebrate IP_3R isoforms, which probably evolved 800 million years ago. Interestingly, the *C. owczarzaki* IP_3R is not activated by Ca^{2+} that activates vertebrate IP_3R, although important residues that coordinate with JD-Ca^{2+} (E1882, E1946, Q1949, and T2581 in hIP_3R3) are all conserved. Phylogenic analyses demonstrated that IP_3R genes should predate RyR genes because Bikonta cells have IP_3R but not RyR genes (117). These findings suggest that the Ca^{2+}-induced Ca^{2+} release function common among IP_3R and RyR was acquired during the evolution between Holozoa and vertebrates.

ENSEMBLE OF IP_3-BOUND STATES IN THE TETRAMERIC IP_3R

Given the lack of cooperativity of IP_3-binding events in the tetramer (79, 118), each subunit would behave independently. Therefore, the conformations of four subunits in the tetrameric channel structure is probably stochastic due to the number of bound IP_3 molecules. Strong evidence for stoichiometry recently showed that the tetrameric IP_3R requires four IP_3 molecules to open the channel (119). The diverse states of IP_3-bound conformations in the tetrameric IP_3R were

recently revealed by three-dimensional classification using cryo-EM (**Figure 2*e***) (85). The location of the HD2/ARM2 domain was variable in these states, and showed a 17-Å shift, consistent with the large-scale motion predicted by comparing cryo-EM structure with X-ray crystal structure (112). Importantly, global conformational changes from IP_3-binding sites to near the channel domain were shown in fourfold symmetry structure, of which four IP_3-binding sites were fully occupied with IP_3. In these conformations, the α-helical domain near IP_3-binding sites moves relative to the β-domain ring stabilized by the HS-loop including Y167/W168. This structural change is consistent with the proposed global conformational changes from the IP_3-binding site to the channel domain (112). The five states of IP_3-bound IP_3R suggest that the structural trajectory concerted movements upon IP_3 binding; local conformational change near the IBC, coupled with movement of the large curvature helical domains that results in a 5° rotation of the JD-Ca^{2+} site, and a 17-Å movement of HD2/ARM2, which coordinates with the CD-Ca^{2+} at the interface with HD1/central linker domain (85). The HD2/ARM2 domain could move in each subunit because the cryo-EM data show asymmetric tetramers; the four IP_3-binding sites are even occupied (**Figure 2*e***). The possible conformational changes in Ca^{2+}-binding sites by IP_3 suggest that IP_3 binding should presumably cooperate with the JD and CD Ca^{2+}-binding activities.

Cryo-EM also revealed the 4.1-Å structure of rat IP_3R1 bound to an IP_3 analogue and adenophostin A, a metabolite that was discovered in *Penicillium breviocompactum* as a potent agonist of IP_3R (120). This demonstrates the ligand-induced conformational changes within the IBC, which are basically consistent with the conformational changes on IP_3 binding (83). The presence of 100 nM of adenophostin A and 300 nM of Ca^{2+} activates IP_3R channels, but no opening of a Ca^{2+} pore gate was determined in the cryo-EM. In the *apo*-state, the diameter of the selective filter was too large to select hydrated ions, but the diameter of adenophostin A-IP_3R1 was narrow enough to accomplish this. In this report, the authors obtained no Ca^{2+} matching density near the site corresponding to the JD Ca^{2+}-binding site and no sufficient dilation to allow a hydrated Ca^{2+} ion to pass through (83). Therefore, the ways in which adenophostin A and Ca^{2+} can cooperate to open the Ca^{2+} channel remain unclear.

Long-Range Allosteric Coupling from IP_3 to Ca^{2+} Gates

The aforementioned structural studies demonstrated several conformations bound to IP_3, Ca^{2+}, and adenophostin A, but the structures of opened channels were never obtained. To discuss the mechanism of channel opening, we should consider not only structures but also functional data. In the past 30 years, two models for the gating mechanism were proposed: One is that the IBC and SD directly bind to the channel domain for gating (121), whereas the other is long-distance coupling from the IBC to the channel (81, 122). Recently, the latter long-distance allosteric coupling theory was supported by cryo-EM analyses, which demonstrated that the IBC/SD is located ~90 Å away from the Ca^{2+} conducting gate. Cryo-EM has showed direct contacts of a C-terminal domain through a long helical bundle connecting to the sixth pore-forming transmembrane helix (84), so the authors proposed that the IBC should directly move the C-terminal helical bundles to open the channel. However, functional analyses of IP_3R1 did not indicate that the IP_3R function was impaired by the deletion of C-terminal residues that directly bind to the IBC in the cryo-EM structure (112, 123). Moreover, a chimera IP_3R swapped with the C-terminal region of RyR, which has no homology with IP_3R C-terminal domain, can release Ca^{2+} in response to IP_3 (92). On the basis of these functional data, contact of the IBC to C-terminal helices should not be essential for the IP_3-dependent gating mechanism. Undoubtedly, the C-terminal coiled regions near the C terminus, which has no contact with the IBC/SD in the cryo-EM, should be pivotal for tetramer formation and/or domain interaction, as indicated by previous reports (123, 124).

The mutagenesis of full-length mouse IP_3R1 has revealed the small structure constructed by 21 amino acid residues, referred to as the leaflet (**Figure 2**) (112). The leaflet directly contacts a linker domain (83); therefore, this leaflet–linker domain interacting site should be a key functional pathway of allosteric coupling from the IBC to the Ca^{2+} channel. The sequence alignment of IP_3R and RyR indicates that the equivalent leaflet region in the RyR intervenes into the Ca^{2+}- and Zn^{2+}-binding sites in the three-dimensional structure revealed by cryo-EM (104). This finding has been confirmed by a recent study (85) suggesting integrative roles of the leaflet region underlying channel activation. Cryo-EM revealed that Ca^{2+} coordinates with side chains of four amino acid residues in RyR, corresponding to E1977, H1979, E2041, and Q2044 residues in IP_3R1. This was confirmed by a recent study in which the atomic density of JD Ca^{2+} was obtained in this binding site (85). Considering the essential role of the E2100 residue in the Ca^{2+} dependent activation (116), we can suppose that this JD Ca^{2+} binding site should be essential for channel opening by IP_3. In the RyR, the Zn^{2+}-binding pocket constructed by critical residues corresponding to C2610 and C2613 residues in IP_3R1 is conserved in the IP_3R of all unicellular and multicellular organisms. The functional role of Zn^{2+} ions in the IP_3R remains largely unknown, but a mutagenesis study demonstrated a complete loss of IP_3R function with a C2610 or C2613 mutation (79), suggesting that Zn^{2+} may be an essential cofactor for stabilizing the structure around these residues; this is referred to as the gatekeeper domain (79). Therefore, this leaflet region linking the regulatory/coupling and channel domains should transmit the IP_3-dependent conformational changes to the Ca^{2+} channel. This idea is also supported by an X-ray crystallography study that demonstrated how IP_3 physically opens the Ca^{2+} channel over a long distance (112). During activation of IP_3R, the movement of the leaflet region could shift the pore-forming transmembrane helix to open the Ca^{2+} pore consequently. In particular, the face of the leaflet contacting the linker domain contains highly conserved isoleucine (I2195), glutamate (E2196), and isoleucine (I2197) residues in IP_3R of all isoforms, various animals, and all known unicellular organisms, including *T. cruzi* and *T. brucei*. Thus, this region is a plausible candidate for mediating the allosteric gating transmission to the channel domain.

Importantly, the IP_3 never opens the channel of IP_3R without Ca^{2+}. Previous functional analysis indicates that a low Ca^{2+} level acts as an essential coagonist for IP_3-gated Ca^{2+} release (9, 10). The requirement of dual ligands is an important basis for signaling cross talk between IP_3 signaling and Ca^{2+} signaling. However, global conformational changes by IP_3 can be induced by IP_3 only and require no Ca^{2+}, as suggested by X-ray crystallography and cryo-EM studies (81, 85). In this case, we suggest that IP_3 can cause global structural changes, but the channel cannot open (**Figure 2*f***, top). By contrast, Ca^{2+} concentration is sufficient to bind to the JD Ca^{2+} binding site near the leaflet, and Ca^{2+} binding should stabilize the spatial configuration between regulatory/coupling and channel domains to efficiently transmit a force from the IBC to the channel (**Figure 2*f***, middle). In the presence of high Ca^{2+}, CD Ca^{2+} stabilizes the HD2/ARM2 domains and induces the large-scale structural changes associated with broken interaction between subunits (81, 85) (**Figure 2*f***, bottom). In this structure, locally IP_3-dependent conformational changes take place, but the fixed end formed at the subunit interface is broken, and the torque force from IBC should still show no transmission to the channel via the leaflet region, even though IP_3 is produced in the cell. The structural basis of the activation mechanism by Ca^{2+} is quite important, warranting further investigation.

REGULATORY MECHANISMS OF IP_3R

To understand the IP_3R regulatory mechanisms, we mapped the known sites for binding proteins (**Figure 3*a***), posttranslational modifications (**Figure 3*b***), and mutations causing human brain

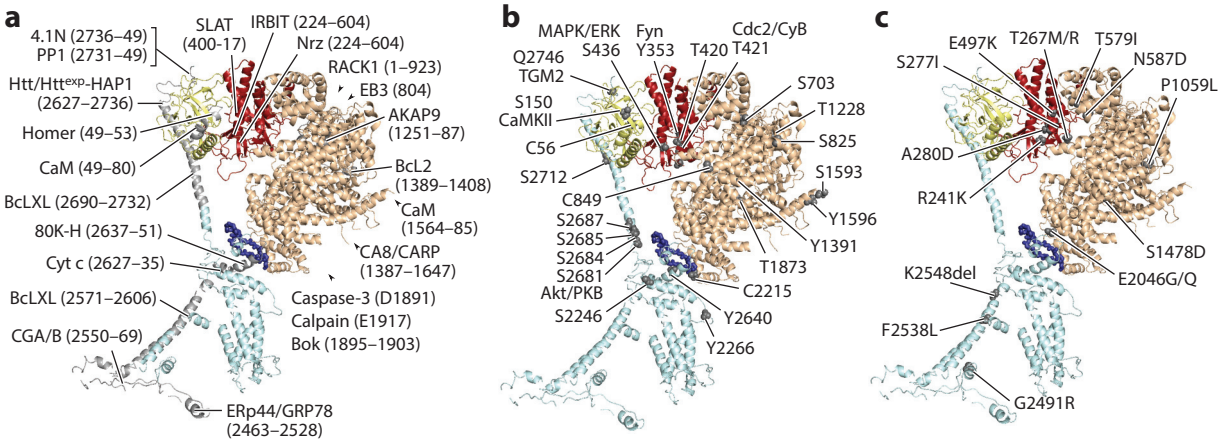

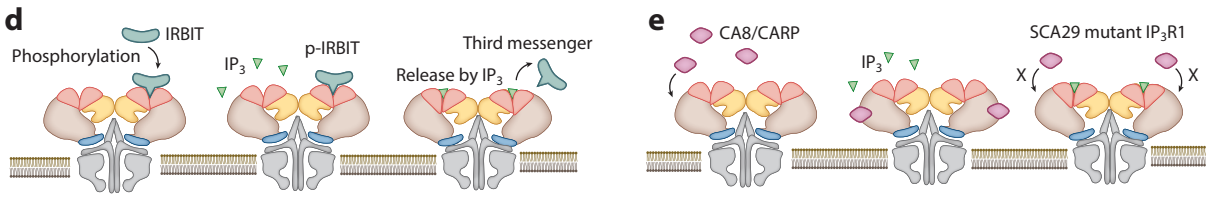

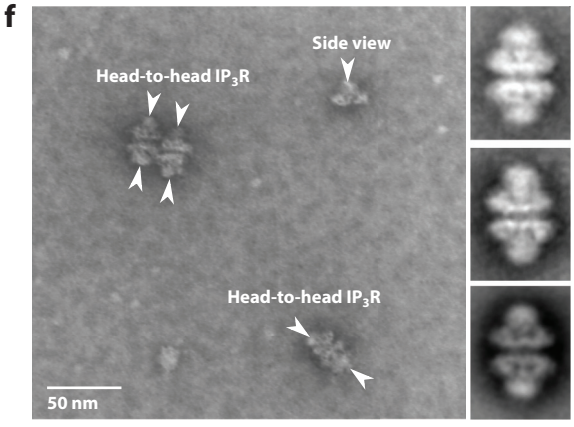

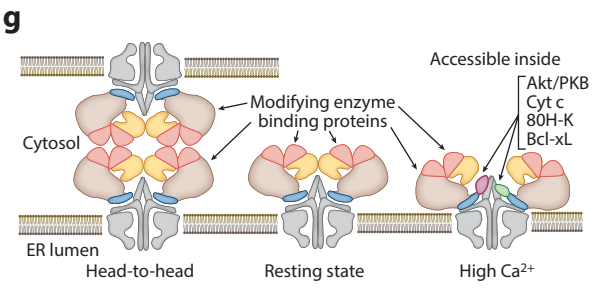

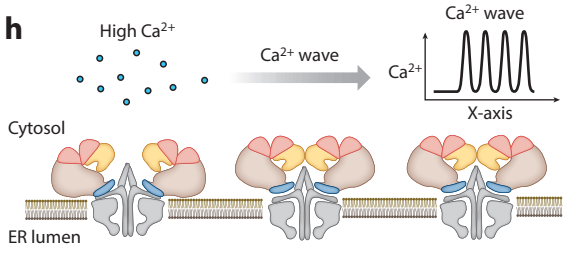

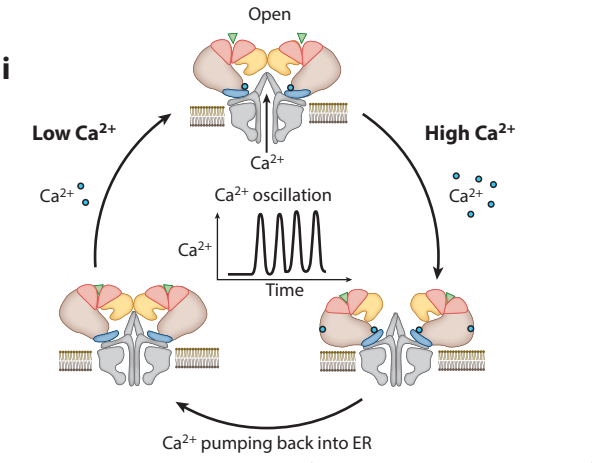

(Caption appears on following page)

Figure 3 (*Figure appears on preceding page*)

Model for IP_3R plasticity. The map of the sites for binding proteins (*a*), posttranslational modifications (*b*), and mutations in genetic diseases (*c*). Amino acid numbers in panels *a* and *b* are represented in the number of mouse IP_3R1 (P11881), and those in panel *c* are shown in the number of human IP_3R1 isoform 2 (splicing sites SI, SII, SIII) (NP_002213.5). (*d–i*) Structural plasticity in IP_3R assembly. We propose structural plasticity that involves dynamic structural changes of IP_3R assembly, including transformation of IP_3R itself and association/dissociation of binding proteins. (*d*) P-IRBIT and IP_3R form a complex and (*e*) IP_3 dissociates it. CA8/CARP and IP_3R form a complex, but the SCA29 mutant IP_3R cannot build it because the mutant cannot bind to CA8/CARP (94). (*f*) In the stacked endoplasmic reticulum (ER), IP_3R makes head-to-head structures. The micrograph of negatively stained IP_3R1 was obtained by electron microscopy. Each arrow indicates a particle of tetrameric IP_3R1. In boxes to the right, characteristic class averages of head-to-head IP_3R1 are shown. (*g*) A model for transformations of IP_3R. On the left is a head-to-head arrangement of tetrameric IP_3R. Ca^{2+}-dependent structural changes that should enable binding proteins and/or modifying enzymes to access inside IP_3R. (*h*) Ca^{2+} waves and Ca^{2+} oscillation (*i*) should determine structural plasticity of IP_3R at each microdomain.

diseases (**Figure 3*c***) in the IP_3R1 structural model. Cytochrome c (cyt c), a mitochondrial hemoprotein involved in the electron transfer system, is released during mitochondria-dependent apoptosis and binds proximally to the leaflet region (125, 126), suggesting that cyt c should affect the leaflet-mediated gating transmission. Another important regulator, Bcl-xL (127), also binds near the leaflet region. A recent report showed that in biphasic regulation, the low concentrations of Bcl-xL activated the channel, whereas high concentrations inhibited it; furthermore, Bcl-xL bound to two distinct sites, H1 (residues 2,571–2,606) and H4 (residues 2,690–2,732) (128). Near the leaflet region is also a target area for alternative splicing variants of the α isoform of the transient receptor potential 4 (αhTRP4) channel but of the other isoform βhTRP4 channel, which associates with the C terminus of IP_3R (residues 2,556–2,713 of IP_3R1) (129). C2214 of rat IP_3R1 is one of the three candidates for the palmitoylation site as the triple mutations (C56A/C849A/C2214A) reduced palmitoylation to 25% in wild-type IP_3R1 and impaired Ca^{2+} release by T cell receptor stimulation in Jurkat T cells (130). The palmitoyl acyl transferase enzyme interacting with Selk proteins would catalyze palmitoylation (130). The S2681 residue of IP_3R1 is phosphorylated by protein kinase B, which is known as Akt kinase (**Figure 3*b***); this phosphorylation should suppress Ca^{2+} release from IP_3R because the S2681A mutant increased the Ca^{2+} release and the mitochondrial Ca^{2+} uptake and apoptosis (131), and staurosporine-induced caspase-3 activation in the S2681A mutant was more significant than in the wild-type or S2681E mutant (132). Around this site, S2684, S2685, S2687, and S2712 of mouse IP_3R1 were phosphorylated as determined by mass spectrometry and shown in a database for phosphorylation (133). S2246 located near the leaflet was phosphorylated (134), and T2056, Y2640, and Y2266 of mouse IP_3R1 could be phosphorylated (133). Interestingly, these sites should be accessible for the modifying enzymes, but how they will affect IP_3R function and apoptosis remains elusive. In human genetic diseases, previous reports demonstrated mutations in the IP_3R (**Figure 3*c***), and major mutation sites are located at the IBC to impair the IP_3-binding activity, as shown recently (94). The E2046 residue is substituted to G or Q [E2094G/Q in hIP_3R1 (NP_001161744.1)] in Gillespie syndrome (135). A three-base-pair deletion at K2548 showed no IP_3R function as measured in the triple knockout cells lacking IP_3R1–3 (136). The mutation of F2538L [F2552L in the hIP_3R1 (NP_001093422.2)] has no functional characterization, but it might impair IP_3R function (136). The mutations of E2046 or its presence outside the IBC should affect allosteric gating transmission, whereas the G2491R residue [G2539R in the hIP_3R1 (NP_001161744.1)] at the Ca^{2+} pore should result in failure of Ca^{2+} permeation (135).

Among known binding partners, only P-IRBIT competitively inhibits IP_3 binding (**Figure 3*a***). P-IRBIT binds to the IP_3-binding site via 10 critical amino acid residues that coordinate with a phosphorous group of IP_3 between the β- and α-rich domains and prevents IP_3 from accessing the binding pocket. P-IRBIT itself has never behaved as an agonist (137); therefore, negative charges

of the phosphate groups in the disordered region of P-IRBIT (137) and a Long-IRBIT splicing variant (138) are probably attracted to the critical residues with positive charges but could not stabilize these conformations to open the channel, similar to a nonspecific inhibitor, heparin. The IP_3-binding core is also a target for a Bcl-2-like 10 (Nrz) that is required for Ca^{2+} signaling during epiboly and gastrulation in zebrafish (139) (**Figure 3*a***). The Nrz protein requires E255 but not the critical amino acid residues for IP_3 binding and molecular docking simulation, suggesting that E255 of zebrafish IP_3R1 most likely contacts Nrz C20. Because the Nrz protein inhibits the IP_3-binding activity, the Nrz should affect the conformational dynamics or stability around the interface between β- and α-rich domains in a different manner from P-IRBIT. In contrast to inhibition by P-IRBIT and Nrz, the guanine nucleotide exchange factor SWAP-70-like adaptor of T cells (SLAT) activated IP_3R1 in T cells by binding to the IP_3-binding domain (140). Disruption of the SLAT-IP_3R1 interaction inhibited T cell receptor–stimulated Ca^{2+} signaling, activation of the transcription factor called nuclear factor of activated T cells (NFAT), and production of cytokines, suggesting that this interaction is required for T cell activation. The critical site for SLAT binding (residues 400–417) (**Figure 3*a***) is near the IP_3-binding pocket and the interface between subunits. Thus, SLAT would facilitate the IP_3-mediated conformational change and/or stabilize the subunit interface. These proteins should differentially regulate IP_3R function, raising the question of how they affect dynamic changes and/or stability in the IBC by an induced fit mechanism and/or conformational selection during IP_3-binding events. Homer (141) and CaM (142) also bind to the SD region (**Figure 3*a***). Many other proteins, such as receptor of activated protein C kinase 1 (RACK1) (7), EB3 (143), AKAP9A-kinase anchor protein 9 (AKAP9) (144), Bcl-2 (145), CaM (146), carbonic anhydrase-related protein (CA8/CARP) (147), caspase-3 (148), calpain (149), and Bok (150), bind to the large regulatory/coupling domain (**Figure 3*a***), suggesting the regulation of conformational status within this domain to control the allosteric gating. The SCA29 mutation of V1538M within the CA8/CARP-binding site of IP_3R1 completely eliminated its interaction with CA8 and CA8-mediated IP_3R1 inhibition. Furthermore, pathological mutations in CA8/CARP decreased CA8/CARP-mediated suppression of IP_3R1 by reducing the interaction with IP_3R1 (94). These results suggest the mechanisms by which pathological mutations cause aberrant assembly changes in IP_3R1.

CA8/CARP: carbonic anhydrase-related protein

Residue S436 of IP_3R1 is phosphorylated by a mitogen-activated protein kinase (MAPK)/extracellular signal–regulated kinase (ERK) pathway (151, 152), which enhances the activity of IP_3R1 (152). This site at the transitional zone from β- and α-rich domains faces to the inside of tetrameric IP_3R (83) (**Figure 3*b***). Thus, this modification requires conformational changes to expose it to the surface. Around the IBC, Y353 is exposed to the surface and phosphorylated by Fyn kinase (153), T420 (154) is located in the IBC, and the SD contains a S150 phosphorylation site and presumed palmitoylation site C56. Two phosphorylation sites, S421 and T799, are phosphorylated by cyclin-dependent kinase (Cdc2/CyB), which increases the IP_3-binding activity (155). S421 is close to Y353 and exposed to the top surface; T799 (equivalent to T795 in IP_3R3) is close to the CD-Ca^{2+} site (85). Phosphorylation of S150 by CaMKII, but not the S150A mutant, leads to inhibition of IP_3R channel activity, and a phosphomimetic mutant S150E exhibits a constitutively low open probability (156). The S150 residue is not exposed to the surface (83, 85), suggesting that CaMKII requires conformational changes in IP_3R. The S703 residue located in the regulatory/coupling domain (HD1) is phosphorylated (157). The regulatory/coupling domain is also phosphorylated at the amino acid residues equivalent to S825, S1228, S1593 (158), Y1391 (159), Y1596, and T1873 (133) in the mouse IP_3R1. In addition to these phosphorylation sites, the ubiquitination (160, 161) and acetylation (162) of lysine residues were also reported in the IP_3R, although the roles of major parts of these sites were uninvestigated. In cells expressing the T930A mutant, IP_3R function and IP_3 binding affinity are activated more than the wild-type

receptors, whereas cells expressing the T930E mutant oppositely show a decreased Ca^{2+} release in response to IP_3 uncaging (163). The Ca^{2+} content in ER is due to a modest overexpression of IP_3R1 and a threefold increased phosphorylation of IP_3R1 on S1716, a protein kinase A consensus site, is implicated in the ER Ca^{2+} leak (164). Glycogen synthase kinase 3β should modify S1756 and regulates mitochondrial Ca^{2+} transfer via IP_3R at the MAM (165). These phosphorylation sites within the regulatory/coupling domain (equivalent to T945 and S1755 of mouse IP_3R) are involved in important functions, but their X-ray crystal or cryo-EM structures remain unknown.

Causative mutation sites in spinocerebellar ataxia and related diseases are localized near the IP_3-binding site at the interface between the β- and α-rich domains and in the α-helical domain (**Figure 3*c***), including four residues of human IP_3R1: R241K (166), T267M/R (167, 168), S277I (168), and A280D (166). Human E497K (166) (equivalent to E512 of mouse IP_3R1) is next to the critical residue R511 of mouse IP_3R1, which coordinates with the phosphorus group of IP_3 (80). Human T579I (168) and N587D (169) are neighboring the helix binding with the phosphorus group of IP_3 (80). Human P1059L (170) (equivalent to P1049 of rat IP_3R1) is located at the HD1/ARM2 of regulatory/coupling domains (83). The P1059L mutation resulted in higher IP_3-binding affinity than the wild type (171), suggesting that the P1059L mutation should affect the structure around the IP_3-binding pocket at a distance. The S1478D mutation (172) is located at the edge of HD3/ARM3 distal from the HD1/ARM2 domain, and V1538M [V1547M in hIP_3R1 (NP_00161744.1)] (169) lies at the region with unsolved structure. Interestingly, IP_3R1 function was impaired by almost all SCA29 mutations but not by CA8/CARP-related S1478D and V1538M mutants (94), suggesting that the SCA29 disease should occur by two different mechanisms in the IP_3R1.

PROPOSED IP_3R PLASTICITY UNDERLYING DIVERSE FUNCTIONS

The recent progress in cryo-EM and X-ray crystallography have strongly contributed to understanding the *apo*-state or IP_3/Ca^{2+}-bound state. Static views of these structures are important for considering the abovementioned regulation by binding partners, posttranslational modifications, and genetic mutations in IP_3R. Moreover, they teach us regulation mechanisms of how binding partners control IP_3R and how enzymes directly modify buried residues. To provide a framework for elucidating regulation of the IP_3R in various cell types, we propose here a model for protein plasticity within IP_3R (**Figure 3*d–i***). This concept is based on the diverse conformational changes of IP_3R per se, a large number of binding proteins, and various posttranslational modifications. We also define that protein plasticity includes allosteric gating and structural changes by IP_3 or Ca^{2+}, which can confer a discrete function to each IP_3R assembly at each cellular microdomain. Importantly, the proposed IP_3R plasticity is also supported by the fact that transglutaminase enzymatically locks the conformation to impair IP_3R functions by cross-linking between subunits (173); that is, plasticity should be necessary for functions. Our proposed concept indicates that the signaling hub of IP_3R itself can be transformable due to spatiotemporal signaling at microdomains for short or long periods.

Given the function of IP_3R at the MAM or ER-PM, the IP_3R at ER-ER contact sites should regulate certain functions, such as Ca^{2+} transport from ER to mitochondria, or other functions, such as a scaffold of IP_3R binding proteins. In the IP_3R tetramer, the top surface of IP_3R should be accessible so that binding proteins, including P-IRBIT, Nrz, SLAT, Homer, CaM, RACK1, EB3, and Sig-1R near the MAM, would easily access but compete for their binding sites. Binding efficiency should be due to the structure of IP_3R assembly. In particular, the IP_3R assembly with P-IRBIT is controlled by IP_3, and local IP_3 signaling including production and diffusion should determine the structure of individual IP_3R assembly (**Figure 3*d***). hTRP3 at the PM associates

with human IP_3R3 through two sites (174), which are located in the regulatory/conduction domain, suggesting that these associations should be dependent on structural states of IP_3R assembly at PM-ER contact sites. Several phosphorylation sites, including Y353 and S150, are located at the top of IP_3R tetramers (**Figure 3*b***), so this phosphorylation should be also affected by the status of IP_3R assembly. In the case of CA8/CARP, formation of the IP_3R-CA8/CARP complex is dependent on the point mutation (**Figure 3*e***). This genetic mutation in IP_3R should affect the protein plasticity of IP_3R-CA8/CARP assembly and is probably critical for the cerebellar ER, where both IP_3R and CA8/CARP are enriched. These structural modifications that occur through binding proteins, modifying enzymes, and generating genetic mutations should locally or temporally determine each assembly structure and result in rapid or chronic protein plasticity at cellular microdomains. Ubiquitination is also an important posttranslational modification of IP_3R at the microdomains. Recent studies have clearly demonstrated that ubiquitin-regulated IP_3R3 plasticity could control IP_3R3 functions at the microdomain (175, 176), probably near the MAM, indicating its role in cancer cell apoptosis. The F-box protein FBXL2 binds IP_3R3, and the PTEN competes with FBXL2 for IP_3R3 binding. These assembly structures control proteasome-mediated degradation to limit Ca^{2+} flux from ER into mitochondria (176). BRCA1-associated protein 1 (BAP1), a potent tumor suppressor gene product, localizes at the ER and binds to deubiquitinate IP_3R3; consequently, BAP1 modulates Ca^{2+} release from the ER into mitochondria to promote apoptosis (175).

IP_3R assembly is formed not only by binding proteins but also by IP_3R itself, according to actual images of purified IP_3R visualized by early EM studies (81, 106). A view with twofold symmetry represents the first true side view of the IP_3R (81) and indicates the presence of a head-to-head state of IP_3R (**Figure 3*f***); the head-to-head structure was sensitive to Ca^{2+}. The dimensions of head-to-head assembly are consistent with the suggested structures at ER-ER membrane contact sites (23, 59–62). How the head-to-head assembly forms with the twofold symmetry is unknown, but we suggest that a specific mechanism should form this ordered binding interface to act at the ER-ER membrane contact sites. This large-scale protein plasticity of IP_3R assembly should confer peculiar functions at the microdomain.

Early observations of purified IP_3Rs also provided real images of the windmill-shaped tetramers of IP_3R1 and demonstrated that relative amounts of windmill structures were dependent on Ca^{2+} (81). A recent cryo-EM study clarified the molecular mechanism at atomic resolutions (85). The phosphorylation of S2681 located at the inner helical bundle (**Figure 3*b***) was also enhanced by Ca^{2+} (113), suggesting that the Akt/PKB kinase could efficiently access the S2681 residue to the Ca^{2+}-bound conformations. The other protein-binding sites for cyt c, Bcl-xL, and other modification sites around the leaflet may be inaccessible for these associating proteins and modifying enzymes in the structure in the absence of Ca^{2+} (**Figure 3*g***). The sites of functional phosphorylation by CaMKII and MAPK/ERK pathways also face to the inside of tetramer. These facts cannot be explained without large-scale structural plasticity in IP_3R. The Ca^{2+}-bound windmill state is a disadvantage for gating transmission, as the ring structure with β-rich domains that should serve as a fixed point during allosteric gating transmission is disrupted. However, this transformation by Ca^{2+} should be reversible (106), and thus modification or binding proteins should reversibly affect IP_3R functions. In particular, the cyt c bound to IP_3R should be released from mitochondria (125, 126), and Bcl proteins should localize at the surface of the mitochondrial membrane (127, 128); therefore, these associations should be mainly assembled near the MAM microdomain. Experimental data demonstrated that nonfunctional IP_3R with Ca^{2+} pore mutations (177) or with deletion of large cytosolic domains, including IP_3-binding sites (177), could regulate staurosporine-induced apoptosis in chicken B cells. Therefore, the high Ca^{2+} state with

inactivated IP_3-induced Ca^{2+} release should present discrete functions in the regulation of apoptotic processes.

Our proposed IP_3R plasticity can aid in adapting individual functions at each microdomain, and spatiotemporal IP_3 or Ca^{2+} signaling at the microdomain should dynamically regulate the incidence of IP_3R plasticity. In the past 20 years, genetically encoded protein indicators were developed for monitoring spatiotemporal patterns of IP_3 and Ca^{2+} concentrations in numerous cell types. Although the mechanism of these dynamics should be probably due to the cell types or stimulants (178), the spatiotemporal dynamics of IP_3 and Ca^{2+} concentrations play important roles in regulating diverse functions, including gene expression, synaptic plasticity, fertilization, and cell death (6, 8). Considering its intrinsic property, IP_3R plasticity should be regulated by the spatiotemporal pattern of local IP_3 and Ca^{2+} concentrations. Previous studies on Ca^{2+} signaling have demonstrated Ca^{2+} puffs (179) and Ca^{2+} wave phenomena (178, 180). This polarized and spatially defined Ca^{2+} signaling could determine the cellular distribution of Ca^{2+}-dependent plasticity in IP_3R (**Figure 3*b***), as Ca^{2+}-dependent structural changes in IP_3R requires no IP_3 (81, 106). During Ca^{2+} oscillation evoked by IP_3, IP_3R should change into at least three states (**Figure 3*i***). In the presence of low Ca^{2+}, Ca^{2+} can bind to a high-affinity Ca^{2+} sensor site or a JD-Ca^{2+} site (**Figure 2*a*** and ***d***); IP_3 can also bind to IP_3R, which could release Ca^{2+}. However, once Ca^{2+} concentrations could reach sufficiently high levels to bind to low affinity sites, most likely CD-Ca^{2+} sites, this high Ca^{2+} relocates HD2/ARM2 domains and causes an opening of the β-ring structure and closure of the Ca^{2+} channel gate by a flapping motion (106), as indicated by cryo-EM (85). Then, the concentration would be decreased by pumping back to the ER or out of cells, and the structure would transform into the resting state because the Ca^{2+}-dependent conformational changes are reversible (106). Thus, it is conceivable that temporal dynamics in IP_3R structures should occur under recurrent Ca^{2+} oscillation, and oscillatory dynamics should provide the incidence of rearrangements in IP_3R assembly at local microdomains. The property of oscillatory changes of Ca^{2+} concentration could determine biological consequences; for example, Ca^{2+} oscillation determines gene expression (181, 182), and temporal patterns of Ca^{2+} oscillation should determine cell apoptosis (183). The temporal pattern of Ca^{2+} concentrations should also determine the temporal behavior of IP_3R structures that could affect the accessibility of binding proteins and modifying enzymes. Importantly, IP_3R plasticity could determine not only the association of these regulatory molecules but also the dissociation of binding molecules regulated by these Ca^{2+} and/or IP_3 temporal patterns. In this case, the dissociated molecules could be considered presumable third messengers, such as P-IRBIT. These properties of protein plasticity within IP_3R may confer an ability to regulate cellular plasticity in response to various cellular stimuli.

CONCLUSION

In the past 40 years, from its discovery to recent research progress, numerous studies have demonstrated that IP_3R mediates diverse functions at cellular microdomains, and its aberrant regulation results in a variety of human diseases. IP_3R genes and IP_3-mediated gating mechanisms already existed when multicellular organisms evolved from unicellular ancestors 800 million years ago, and these primitive genes have subsequently evolved into three vertebrate isoforms. In mammals, further translational variants have since evolved, and posttranslational modifications and binding proteins have added further dimensions to mammalian IP_3R regulation. This increasing regulation of IP_3R probably conferred plasticity to IP_3R in order to adapt to diverse environments at cellular microdomains of pathophysiological states. The structures of IP_3R determined by recent emerging structural analyses, including cryo-EM and X-ray crystallography, provide a new structural basis for allosteric gating to understand the core mechanism of IP_3-gated Ca^{2+} release and

a new conceptual framework for protein plasticity underlying diverse functions in ligand-gated ion channels and other functional proteins. The next steps should be to observe these protein dynamics in action to decipher the regulatory mechanisms deeply. Our proposed concept of IP_3R plasticity should not only explain how binding partners or enzymes can target inaccessible sites but also provide a mechanistic basis for the specific function regulated by spatiotemporal IP_3 and Ca^{2+} signaling at each microdomain. To observe such protein dynamics, concrete cellular examples are needed. In particular, knowledge of protein plasticity will require high-quality assessment of protein components and posttranslational modification of protein assembly at each microdomain. In the future, empirical observations of dynamic motions in action will require new imaging technologies, and analyses of molecular behavior at the microdomains will be necessary to better understand the physiological roles of structural plasticity at discrete microdomains. We suggest that these structural plasticity mechanisms triggered by dynamic transformations of the IP_3R assembly at each microdomain, including Ca^{2+}-dependent regulation, binding proteins, and posttranslational modifications, are involved in state-dependent properties of locally diverse functions. In case of differentiated and polarized cells, we can assume that these protein mechanisms presumably control local plasticity at cellular microdomains in many bodily organs, including the brain.

DISCLOSURE STATEMENT

The authors are not aware of any affiliations, memberships, funding, or financial holdings that might be perceived as affecting the objectivity of this review.

ACKNOWLEDGMENTS

K.H. was supported by the Japan Society for the Promotion of Science Grants-in-Aid for Scientific Research C (15K06791) and Innovative Areas (Brain Protein Aging and Dementia Control; 17H05711). K.M. was supported by Scientific Research S (25221002) from the Japan Society for the Promotion of Science; and by ICORP/ICORP-SORST from the Japan Science and Technology Agency.

LITERATURE CITED

1. Mikoshiba K, Changeux JP. 1978. Morphological and biochemical studies on isolated molecular and granular layers from bovine cerebellum. *Brain Res.* 142:487–504
2. Mikoshiba K, Huchet M, Changeux JP. 1979. Biochemical and immunological studies on the P_{400} protein, a protein characteristic of the Purkinje cell from mouse and rat cerebellum. *Dev. Neurosci.* 2:254–75
3. Crepel F, Dupont JL, Gardette R. 1984. Selective absence of calcium spikes in Purkinje cells of staggerer mutant mice in cerebellar slices maintained in vitro. *J. Physiol.* 346:111–25
4. Maeda N, Niinobe M, Nakahira K, Mikoshiba K. 1988. Purification and characterization of P_{400} protein, a glycoprotein characteristic of Purkinje cell, from mouse cerebellum. *J. Neurochem.* 51:1724–30
5. Furuichi T, Yoshikawa S, Miyawaki A, Wada K, Maeda N, Mikoshiba K. 1989. Primary structure and functional expression of the inositol 1,4,5-trisphosphate-binding protein P_{400}. *Nature* 342:32–38
6. Foskett JK, White C, Cheung KH, Mak DO. 2007. Inositol trisphosphate receptor Ca^{2+} release channels. *Physiol. Rev.* 87:593–658
7. Patterson RL, Boehning D, Snyder SH. 2004. Inositol 1,4,5-trisphosphate receptors as signal integrators. *Annu. Rev. Biochem.* 73:437–65
8. Berridge MJ. 2016. The inositol trisphosphate/calcium signaling pathway in health and disease. *Physiol. Rev.* 96:1261–96

9. Iino M. 1990. Biphasic Ca^{2+} dependence of inositol 1,4,5-trisphosphate-induced Ca release in smooth muscle cells of the guinea pig taenia caeci. *J. Gen. Physiol.* 95:1103–22
10. Bezprozvanny I, Watras J, Ehrlich BE. 1991. Bell-shaped calcium-response curves of Ins(1,4,5)P_3- and calcium-gated channels from endoplasmic reticulum of cerebellum. *Nature* 351:751–54
11. Matsumoto M, Nakagawa T, Inoue T, Nagata E, Tanaka K, et al. 1996. Ataxia and epileptic seizures in mice lacking type 1 inositol 1,4,5-trisphosphate receptor. *Nature* 379:168–71
12. Inoue T, Kato K, Kohda K, Mikoshiba K. 1998. Type 1 inositol 1,4,5-trisphosphate receptor is required for induction of long-term depression in cerebellar Purkinje neurons. *J. Neurosci.* 18:5366–73
13. Hisatsune C, Kuroda Y, Akagi T, Torashima T, Hirai H, et al. 2006. Inositol 1,4,5-trisphosphate receptor type 1 in granule cells, not in Purkinje cells, regulates the dendritic morphology of Purkinje cells through brain-derived neurotrophic factor production. *J. Neurosci.* 26:10916–24
14. Hisatsune C, Miyamoto H, Hirono M, Yamaguchi N, Sugawara T, et al. 2013. IP_3R1 deficiency in the cerebellum/brainstem causes basal ganglia-independent dystonia by triggering tonic Purkinje cell firings in mice. *Front. Neural Circuits* 7:156
15. Sugawara T, Hisatsune C, Le TD, Hashikawa T, Hirono M, et al. 2013. Type 1 inositol trisphosphate receptor regulates cerebellar circuits by maintaining the spine morphology of purkinje cells in adult mice. *J. Neurosci.* 33:12186–96
16. Sugawara T, Hisatsune C, Miyamoto H, Ogawa N, Mikoshiba K. 2017. Regulation of spinogenesis in mature Purkinje cells via mGluR/PKC-mediated phosphorylation of CaMKIIβ. *PNAS* 114:E5256–65
17. Tsuboi D, Kuroda K, Tanaka M, Namba T, Iizuka Y, et al. 2015. Disrupted-in-schizophrenia 1 regulates transport of *ITPR1* mRNA for synaptic plasticity. *Nat. Neurosci.* 18:698–707
18. Monai H, Ohkura M, Tanaka M, Oe Y, Konno A, et al. 2016. Calcium imaging reveals glial involvement in transcranial direct current stimulation-induced plasticity in mouse brain. *Nat. Commun.* 7:11100
19. Nizar K, Uhlirova H, Tian P, Saisan PA, Cheng Q, et al. 2013. *In vivo* stimulus-induced vasodilation occurs without IP_3 receptor activation and may precede astrocytic calcium increase. *J. Neurosci.* 33:8411–22
20. Petravicz J, Fiacco TA, McCarthy KD. 2008. Loss of IP_3 receptor-dependent Ca^{2+} increases in hippocampal astrocytes does not affect baseline CA1 pyramidal neuron synaptic activity. *J. Neurosci.* 28:4967–73
21. Sherwood MW, Arizono M, Hisatsune C, Bannai H, Ebisui E, et al. 2017. Astrocytic IP_3Rs: contribution to Ca^{2+} signalling and hippocampal LTP. *Glia* 65:502–13
22. Okubo Y, Kanemaru K, Suzuki J, Kobayashi K, Hirose K, Iino M. 2019. Inositol 1,4,5-trisphosphate receptor type 2-independent Ca^{2+} release from the endoplasmic reticulum in astrocytes. *Glia* 67:113–24
23. Satoh T, Ross CA, Villa A, Supattapone S, Pozzan T, et al. 1990. The inositol 1,4,5,-trisphosphate receptor in cerebellar Purkinje cells: quantitative immunogold labeling reveals concentration in an ER subcompartment. *J. Cell Biol.* 111:615–24
24. Pinton P, Pozzan T, Rizzuto R. 1998. The Golgi apparatus is an inositol 1,4,5-trisphosphate-sensitive Ca^{2+} store, with functional properties distinct from those of the endoplasmic reticulum. *EMBO J.* 17:5298–308
25. Gerasimenko OV, Gerasimenko JV, Tepikin AV, Petersen OH. 1995. ATP-dependent accumulation and inositol trisphosphate- or cyclic ADP-ribose-mediated release of Ca^{2+} from the nuclear envelope. *Cell* 80:439–44
26. Stehno-Bittel L, Perez-Terzic C, Clapham DE. 1995. Diffusion across the nuclear envelope inhibited by depletion of the nuclear Ca^{2+} store. *Science* 270:1835–38
27. Huh YH, Yoo SH. 2003. Presence of the inositol 1,4,5-triphosphate receptor isoforms in the nucleoplasm. *FEBS Lett.* 555:411–18
28. Fadool DA, Ache BW. 1992. Plasma membrane inositol 1,4,5-trisphosphate-activated channels mediate signal transduction in lobster olfactory receptor neurons. *Neuron* 9:907–18
29. Kuno M, Maeda N, Mikoshiba K. 1994. IP_3-activated calcium-permeable channels in the inside-out patches of cultured cerebellar Purkinje cells. *Biochem. Biophys. Res. Commun.* 199:1128–35
30. Echevarria W, Leite MF, Guerra MT, Zipfel WR, Nathanson MH. 2003. Regulation of calcium signals in the nucleus by a nucleoplasmic reticulum. *Nat. Cell Biol.* 5:440–46

31. Bading H. 2013. Nuclear calcium signalling in the regulation of brain function. *Nat. Rev. Neurosci.* 14:593–608
32. Ondrias K, Lencesova L, Sirova M, Labudova M, Pastorekova S, et al. 2011. Apoptosis induced clustering of IP_3R1 in nuclei of non-differentiated PC12 cells. *J. Cell Physiol.* 226:3147–55
33. Ikebara JM, Takada SH, Cardoso DS, Dias NM, de Campos BC, et al. 2017. Functional role of intracellular calcium receptor inositol 1,4,5-trisphosphate type 1 in rat hippocampus after neonatal anoxia. *PLOS ONE* 12:e0169861
34. Khan AA, Soloski MJ, Sharp AH, Schilling G, Sabatini DM, et al. 1996. Lymphocyte apoptosis: mediation by increased type 3 inositol 1,4,5-trisphosphate receptor. *Science* 273:503–7
35. El-Daher SS, Patel Y, Siddiqua A, Hassock S, Edmunds S, et al. 2000. Distinct localization and function of $^{1,4,5}IP_3$ receptor subtypes and the $^{1,3,4,5}IP_4$ receptor $GAP1^{IP4BP}$ in highly purified human platelet membranes. *Blood* 95:3412–22
36. Guillemette G, Balla T, Baukal AJ, Catt KJ. 1988. Characterization of inositol 1,4,5-trisphosphate receptors and calcium mobilization in a hepatic plasma membrane fraction. *J. Biol. Chem.* 263:4541–48
37. Vazquez G, Wedel BJ, Bird GS, Joseph SK, Putney JW. 2002. An inositol 1,4,5-trisphosphate receptor-dependent cation entry pathway in DT40 B lymphocytes. *EMBO J.* 21:4531–8
38. Dellis O, Dedos SG, Tovey SC, Taufiq-Ur-Rahman, Dubel SJ, Taylor CW. 2006. Ca^{2+} entry through plasma membrane IP_3 receptors. *Science* 313:229–33
39. Docampo R, de Souza W, Miranda K, Rohloff P, Moreno SN. 2005. Acidocalcisomes—conserved from bacteria to man. *Nat. Rev. Microbiol.* 3:251–61
40. Lander N, Chiurillo MA, Storey M, Vercesi AE, Docampo R. 2016. CRISPR/Cas9-mediated endogenous C-terminal tagging of *Trypanosoma cruzi* genes reveals the acidocalcisome localization of the inositol 1,4,5-trisphosphate receptor. *J. Biol. Chem.* 291:25505–15
41. Huang G, Bartlett PJ, Thomas AP, Moreno SN, Docampo R. 2013. Acidocalcisomes of *Trypanosoma brucei* have an inositol 1,4,5-trisphosphate receptor that is required for growth and infectivity. *PNAS* 110:1887–92
42. Li FJ, He CY. 2014. Acidocalcisome is required for autophagy in *Trypanosoma brucei*. *Autophagy* 10:1978–88
43. Rizzuto R, Pinton P, Carrington W, Fay FS, Fogarty KE, et al. 1998. Close contacts with the endoplasmic reticulum as determinants of mitochondrial Ca^{2+} responses. *Science* 280:1763–66
44. Csordas G, Renken C, Varnai P, Walter L, Weaver D, et al. 2006. Structural and functional features and significance of the physical linkage between ER and mitochondria. *J. Cell Biol.* 174:915–21
45. Szabadkai G, Bianchi K, Varnai P, De Stefani D, Wieckowski MR, et al. 2006. Chaperone-mediated coupling of endoplasmic reticulum and mitochondrial Ca^{2+} channels. *J. Cell Biol.* 175:901–11
46. Betz C, Stracka D, Prescianotto-Baschong C, Frieden M, Demaurex N, Hall MN. 2013. mTOR complex 2-Akt signaling at mitochondria-associated endoplasmic reticulum membranes (MAM) regulates mitochondrial physiology. *PNAS* 110:12526–34
47. Hamasaki M, Furuta N, Matsuda A, Nezu A, Yamamoto A, et al. 2013. Autophagosomes form at ER-mitochondria contact sites. *Nature* 495:389–93
48. Garvey M, Klose H, Fischer R, Lambertz C, Commandeur U. 2013. Cellulases for biomass degradation: comparing recombinant cellulase expression platforms. *Trends Biotechnol.* 31:581–93
49. Iwasawa R, Mahul-Mellier AL, Datler C, Pazarentzos E, Grimm S. 2011. Fis1 and Bap31 bridge the mitochondria-ER interface to establish a platform for apoptosis induction. *EMBO J.* 30:556–68
50. Cárdenas C, Müller M, McNeal A, Lovy A, Jaňa F, et al. 2016. Selective vulnerability of cancer cells by inhibition of Ca^{2+} transfer from endoplasmic reticulum to mitochondria. *Cell Rep.* 14:2313–24
51. Bonneau B, Ando H, Kawaai K, Hirose M, Takahashi-Iwanaga H, Mikoshiba K. 2016. IRBIT controls apoptosis by interacting with the Bcl-2 homolog, Bcl2l10, and by promoting ER-mitochondria contact. *eLife* 5:e19896
52. Hayashi T, Su TP. 2007. Sigma-1 receptor chaperones at the ER-mitochondrion interface regulate Ca^{2+} signaling and cell survival. *Cell* 131:596–610

53. Brailoiu E, Chakraborty S, Brailoiu GC, Zhao P, Barr JL, et al. 2019. Choline is an intracellular messenger linking extracellular stimuli to IP_3-evoked Ca^{2+} signals through sigma-1 receptors. *Cell Rep.* 26:330–37.e4
54. Petkovic M, Jemaiel A, Daste F, Specht CG, Izeddin I, et al. 2014. The SNARE Sec22b has a non-fusogenic function in plasma membrane expansion. *Nat. Cell Biol.* 16:434–44
55. Fernandez-Busnadiego R, Saheki Y, De Camilli P. 2015. Three-dimensional architecture of extended synaptotagmin-mediated endoplasmic reticulum-plasma membrane contact sites. *PNAS* 112:E2004–13
56. Lur G, Sherwood MW, Ebisui E, Haynes L, Feske S, et al. 2011. InsP_3 receptors and Orai channels in pancreatic acinar cells: co-localization and its consequences. *Biochem. J.* 436:231–39
57. Okeke E, Parker T, Dingsdale H, Concannon M, Awais M, et al. 2016. Epithelial-mesenchymal transition, IP_3 receptors and ER-PM junctions: translocation of Ca^{2+} signalling complexes and regulation of migration. *Biochem. J.* 473:757–67
58. Wang Q, Wang Y, Downey GP, Plotnikov S, McCulloch CA. 2016. A ternary complex comprising FAK, PTPα and IP_3 receptor 1 functionally engages focal adhesions and the endoplasmic reticulum to mediate IL-1-induced Ca^{2+} signalling in fibroblasts. *Biochem. J.* 473:397–410
59. Otsu H, Yamamoto A, Maeda N, Mikoshiba K, Tashiro Y. 1990. Immunogold localization of inositol 1, 4, 5-trisphosphate ($InsP_3$) receptor in mouse cerebellar Purkinje cells using three monoclonal antibodies. *Cell Struct. Funct.* 15:163–73
60. Yamamoto A, Otsu H, Yoshimori T, Maeda N, Mikoshiba K, Tashiro Y. 1991. Stacks of flattened smooth endoplasmic reticulum highly enriched in inositol 1,4,5-trisphosphate ($InsP_3$) receptor in mouse cerebellar Purkinje cells. *Cell Struct. Funct.* 16:419–32
61. Rusakov DA, Podini P, Villa A, Meldolesi J. 1993. Tridimensional organization of Purkinje neuron cisternal stacks, a specialized endoplasmic-reticulum subcompartment rich in inositol 1,4,5-trisphosphate receptors. *J. Neurocytol.* 22:273–82
62. Takei K, Mignery GA, Mugnaini E, Sudhof TC, De Camilli P. 1994. Inositol 1,4,5-trisphosphate receptor causes formation of ER cisternal stacks in transfected fibroblasts and in cerebellar Purkinje cells. *Neuron* 12:327–42
63. Banno T, Kohno K. 1996. Conformational changes of smooth endoplasmic reticulum induced by brief anoxia in rat Purkinje cells. *J. Comp. Neurol.* 369:462–71
64. Ikemoto T, Yorifuji H, Satoh T, Vizi ES. 2003. Reversibility of cisternal stack formation during hypoxic hypoxia and subsequent reoxygenation in cerebellar Purkinje cells. *Neurochem. Res.* 28:1535–42
65. Varadarajan S, Bampton ET, Smalley JL, Tanaka K, Caves RE, et al. 2012. A novel cellular stress response characterised by a rapid reorganisation of membranes of the endoplasmic reticulum. *Cell Death Differ.* 19:1896–907
66. Varadarajan S, Tanaka K, Smalley JL, Bampton ET, Pellecchia M, et al. 2013. Endoplasmic reticulum membrane reorganization is regulated by ionic homeostasis. *PLOS ONE* 8:e56603
67. Morgan AJ, Platt FM, Lloyd-Evans E, Galione A. 2011. Molecular mechanisms of endolysosomal Ca^{2+} signalling in health and disease. *Biochem. J.* 439:349–74
68. Prinz WA. 2014. Bridging the gap: membrane contact sites in signaling, metabolism, and organelle dynamics. *J. Cell Biol.* 205:759–69
69. Elbaz Y, Schuldiner M. 2011. Staying in touch: the molecular era of organelle contact sites. *Trends Biochem. Sci.* 36:616–23
70. Mignery GA, Newton CL, Archer BT 3rd, Sudhof TC. 1990. Structure and expression of the rat inositol 1,4,5-trisphosphate receptor. *J. Biol. Chem.* 265:12679–85
71. Ross CA, Danoff SK, Schell MJ, Snyder SH, Ullrich A. 1992. Three additional inositol 1,4,5-trisphosphate receptors: molecular cloning and differential localization in brain and peripheral tissues. *PNAS* 89:4265–69
72. Yamamoto-Hino M, Sugiyama T, Hikichi K, Mattei MG, Hasegawa K, et al. 1994. Cloning and characterization of human type 2 and type 3 inositol 1,4,5-trisphosphate receptors. *Recept. Channels* 2:9–22
73. Iwai M, Tateishi Y, Hattori M, Mizutani A, Nakamura T, et al. 2005. Molecular cloning of mouse type 2 and type 3 inositol 1,4,5-trisphosphate receptors and identification of a novel type 2 receptor splice variant. *J. Biol. Chem.* 280:10305–17

74. Nakagawa T, Okano H, Furuichi T, Aruga J, Mikoshiba K. 1991. The subtypes of the mouse inositol 1,4,5-trisphosphate receptor are expressed in a tissue-specific and developmentally specific manner. *PNAS* 88:6244–48
75. Danoff SK, Ferris CD, Donath C, Fischer GA, Munemitsu S, et al. 1991. Inositol 1,4,5-trisphosphate receptors: distinct neuronal and nonneuronal forms derived by alternative splicing differ in phosphorylation. *PNAS* 88:2951–55
76. Yamada N, Makino Y, Clark RA, Pearson DW, Mattei MG, et al. 1994. Human inositol 1,4,5-trisphosphate type-1 receptor, $InsP_3R1$: structure, function, regulation of expression and chromosomal localization. *Biochem. J.* 302(Part 3):781–90
77. Regan MR, Lin DD, Emerick MC, Agnew WS. 2005. The effect of higher order RNA processes on changing patterns of protein domain selection: a developmentally regulated transcriptome of type 1 inositol 1,4,5-trisphosphate receptors. *Proteins* 59:312–31
78. Yoshikawa F, Morita M, Monkawa T, Michikawa T, Furuichi T, Mikoshiba K. 1996. Mutational analysis of the ligand binding site of the inositol 1,4,5-trisphosphate receptor. *J. Biol. Chem.* 271:18277–84
79. Uchida K, Miyauchi H, Furuichi T, Michikawa T, Mikoshiba K. 2003. Critical regions for activation gating of the inositol 1,4,5-trisphosphate receptor. *J. Biol. Chem.* 278:16551–60
80. Bosanac I, Alattia JR, Mal TK, Chan J, Talarico S, et al. 2002. Structure of the inositol 1,4,5-trisphosphate receptor binding core in complex with its ligand. *Nature* 420:696–700
81. Hamada K, Terauchi A, Mikoshiba K. 2003. Three-dimensional rearrangements within inositol 1,4,5-trisphosphate receptor by calcium. *J. Biol. Chem.* 278:52881–89
82. Sato C, Hamada K, Ogura T, Miyazawa A, Iwasaki K, et al. 2004. Inositol 1,4,5-trisphosphate receptor contains multiple cavities and L-shaped ligand-binding domains. *J. Mol. Biol.* 336:155–64
83. Fan G, Baker MR, Wang Z, Seryshev AB, Ludtke SJ, et al. 2018. Cryo-EM reveals ligand induced allostery underlying $InsP_3R$ channel gating. *Cell Res.* 28:1158–70
84. Fan G, Baker ML, Wang Z, Baker MR, Sinyagovskiy PA, et al. 2015. Gating machinery of $InsP_3R$ channels revealed by electron cryomicroscopy. *Nature* 527:336–41
85. Paknejad N, Hite RK. 2018. Structural basis for the regulation of inositol trisphosphate receptors by Ca^{2+} and IP_3. *Nat. Struct. Mol. Biol.* 25:660–68
86. Sudhof TC, Newton CL, Archer BT 3rd, Ushkaryov YA, Mignery GA. 1991. Structure of a novel $InsP_3$ receptor. *EMBO J.* 10:3199–206
87. Ida Y, Kidera A. 2013. The conserved Arg241-Glu439 salt bridge determines flexibility of the inositol 1,4,5-trisphosphate receptor binding core in the ligand-free state. *Proteins* 81:1699–708
88. Bosanac I, Yamazaki H, Matsu-Ura T, Michikawa T, Mikoshiba K, Ikura M. 2005. Crystal structure of the ligand binding suppressor domain of type 1 inositol 1,4,5-trisphosphate receptor. *Mol. Cell* 17:193–203
89. Yamazaki H, Chan J, Ikura M, Michikawa T, Mikoshiba K. 2010. Tyr-167/Trp-168 in type 1/3 inositol 1,4,5-trisphosphate receptor mediates functional coupling between ligand binding and channel opening. *J. Biol. Chem.* 285:36081–91
90. Iwai M, Michikawa T, Bosanac I, Ikura M, Mikoshiba K. 2007. Molecular basis of the isoform-specific ligand-binding affinity of inositol 1,4,5-trisphosphate receptors. *J. Biol. Chem.* 282:12755–64
91. Lin CC, Baek K, Lu Z. 2011. Apo and $InsP_3$-bound crystal structures of the ligand-binding domain of an $InsP_3$ receptor. *Nat. Struct. Mol. Biol.* 18:1172–74
92. Seo MD, Velamakanni S, Ishiyama N, Stathopulos PB, Rossi AM, et al. 2012. Structural and functional conservation of key domains in $InsP_3$ and ryanodine receptors. *Nature* 483:108–12
93. Chandran A, Chee X, Prole DL, Rahman T. 2019. Exploration of inositol 1,4,5-trisphosphate (IP_3) regulated dynamics of N-terminal domain of IP_3 receptor reveals early phase molecular events during receptor activation. *Sci. Rep.* 9:2454
94. Ando H, Hirose M, Mikoshiba K. 2018. Aberrant IP_3 receptor activities revealed by comprehensive analysis of pathological mutations causing spinocerebellar ataxia 29. *PNAS* 115:12259–64
95. Ladenburger EM, Korn I, Kasielke N, Wassmer T, Plattner H. 2006. An Ins(1,4,5)P_3 receptor in *Paramecium* is associated with the osmoregulatory system. *J. Cell Sci.* 119:3705–17

96. Hashimoto M, Enomoto M, Morales J, Kurebayashi N, Sakurai T, et al. 2013. Inositol 1,4,5-trisphosphate receptor regulates replication, differentiation, infectivity and virulence of the parasitic protist *Trypanosoma cruzi*. *Mol. Microbiol.* 87:1133–50
97. Hashimoto M, Doi M, Kurebayashi N, Furukawa K, Hirawake-Mogi H, et al. 2016. Inositol 1,4,5-trisphosphate receptor determines intracellular Ca^{2+} concentration in *Trypanosoma cruzi* throughout its life cycle. *FEBS Open Bio* 6:1178–85
98. Morales-Perez CL, Noviello CM, Hibbs RE. 2016. X-ray structure of the human α4β2 nicotinic receptor. *Nature* 538:411–15
99. Zhu S, Stein RA, Yoshioka C, Lee CH, Goehring A, et al. 2016. Mechanism of NMDA receptor inhibition and activation. *Cell* 165:704–14
100. Chen L, Durr KL, Gouaux E. 2014. X-ray structures of AMPA receptor-cone snail toxin complexes illuminate activation mechanism. *Science* 345:1021–26
101. Miller PS, Aricescu AR. 2014. Crystal structure of a human $GABA_A$ receptor. *Nature* 512:270–75
102. Hassaine G, Deluz C, Grasso L, Wyss R, Tol MB, et al. 2014. X-ray structure of the mouse serotonin 5-HT3 receptor. *Nature* 512:276–81
103. Mansoor SE, Lu W, Oosterheert W, Shekhar M, Tajkhorshid E, Gouaux E. 2016. X-ray structures define human $P2X_3$ receptor gating cycle and antagonist action. *Nature* 538:66–71
104. des Georges A, Clarke OB, Zalk R, Yuan Q, Condon KJ, et al. 2016. Structural basis for gating and activation of RyR1. *Cell* 167:145–57.e17
105. Chadwick CC, Saito A, Fleischer S. 1990. Isolation and characterization of the inositol trisphosphate receptor from smooth muscle. *PNAS* 87:2132–36
106. Hamada K, Miyata T, Mayanagi K, Hirota J, Mikoshiba K. 2002. Two-state conformational changes in inositol 1,4,5-trisphosphate receptor regulated by calcium. *J. Biol. Chem.* 277:21115–18
107. da Fonseca PC, Morris SA, Nerou EP, Taylor CW, Morris EP. 2003. Domain organization of the type 1 inositol 1,4,5-trisphosphate receptor as revealed by single-particle analysis. *PNAS* 100:3936–41
108. Jiang QX, Thrower EC, Chester DW, Ehrlich BE, Sigworth FJ. 2002. Three-dimensional structure of the type 1 inositol 1,4,5-trisphosphate receptor at 24 Å resolution. *EMBO J.* 21:3575–81
109. Serysheva II, Bare DJ, Ludtke SJ, Kettlun CS, Chiu W, Mignery GA. 2003. Structure of the type 1 inositol 1,4,5-trisphosphate receptor revealed by electron cryomicroscopy. *J. Biol. Chem.* 278:21319–22
110. Henderson R, Sali A, Baker ML, Carragher B, Devkota B, et al. 2012. Outcome of the first electron microscopy validation task force meeting. *Structure* 20:205–14
111. Henderson R. 2013. Avoiding the pitfalls of single particle cryo-electron microscopy: Einstein from noise. *PNAS* 110:18037–41
112. Hamada K, Miyatake H, Terauchi A, Mikoshiba K. 2017. IP_3-mediated gating mechanism of the IP_3 receptor revealed by mutagenesis and X-ray crystallography. *PNAS* 114:4661–66
113. Anyatonwu G, Khan MT, Schug ZT, da Fonseca PC, Morris EP, Joseph SK. 2010. Calcium-dependent conformational changes in inositol trisphosphate receptors. *J. Biol. Chem.* 285:25085–93
114. Shinohara T, Michikawa T, Enomoto M, Goto J, Iwai M, et al. 2011. Mechanistic basis of bell-shaped dependence of inositol 1,4,5-trisphosphate receptor gating on cytosolic calcium. *PNAS* 108:15486–91
115. Sienaert I, Missiaen L, De Smedt H, Parys JB, Sipma H, Casteels R. 1997. Molecular and functional evidence for multiple Ca^{2+}-binding domains in the type 1 inositol 1,4,5-trisphosphate receptor. *J. Biol. Chem.* 272:25899–906
116. Miyakawa T, Mizushima A, Hirose K, Yamazawa T, Bezprozvanny I, et al. 2001. Ca^{2+}-sensor region of IP_3 receptor controls intracellular Ca^{2+} signaling. *EMBO J.* 20:1674–80
117. Alzayady KJ, Sebe-Pedros A, Chandrasekhar R, Wang L, Ruiz-Trillo I, Yule DI. 2015. Tracing the evolutionary history of inositol, 1,4,5-trisphosphate receptor: insights from analyses of *Capsaspora owczarzaki* Ca^{2+} release channel orthologs. *Mol. Biol. Evol.* 32:2236–53
118. Nunn DL, Taylor CW. 1990. Liver inositol, 1,4,5-trisphosphate-binding sites are the Ca^{2+}-mobilizing receptors. *Biochem. J.* 270:227–32
119. Alzayady KJ, Wang L, Chandrasekhar R, Wagner LE 2nd, Van Petegem F, Yule DI. 2016. Defining the stoichiometry of inositol 1,4,5-trisphosphate binding required to initiate Ca^{2+} release. *Sci. Signal.* 9:ra35

120. Takahashi M, Tanzawa K, Takahashi S. 1994. Adenophostins, newly discovered metabolites of *Penicillium brevicompactum*, act as potent agonists of the inositol 1,4,5-trisphosphate receptor. *J. Biol. Chem.* 269:369–72
121. Boehning D, Joseph SK. 2000. Direct association of ligand-binding and pore domains in homo- and heterotetrameric inositol 1,4,5-trisphosphate receptors. *EMBO J.* 19:5450–59
122. Hamada K, Mikoshiba K. 2012. Revisiting channel allostery: a coherent mechanism in IP_3 and ryanodine receptors. *Sci. Signal.* 5:pe24
123. Schug ZT, Joseph SK. 2006. The role of the S4-S5 linker and C-terminal tail in inositol 1,4,5-trisphosphate receptor function. *J. Biol. Chem.* 281:24431–40
124. Galvan DL, Mignery GA. 2002. Carboxyl-terminal sequences critical for inositol 1,4,5-trisphosphate receptor subunit assembly. *J. Biol. Chem.* 277:48248–60
125. Boehning D, Patterson RL, Sedaghat L, Glebova NO, Kurosaki T, Snyder SH. 2003. Cytochrome *c* binds to inositol (1,4,5) trisphosphate receptors, amplifying calcium-dependent apoptosis. *Nat. Cell Biol.* 5:1051–61
126. Boehning D, van Rossum DB, Patterson RL, Snyder SH. 2005. A peptide inhibitor of cytochrome *c*/inositol 1,4,5-trisphosphate receptor binding blocks intrinsic and extrinsic cell death pathways. *PNAS* 102:1466–71
127. White C, Li C, Yang J, Petrenko NB, Madesh M, et al. 2005. The endoplasmic reticulum gateway to apoptosis by Bcl-X_L modulation of the $InsP_3R$. *Nat. Cell Biol.* 7:1021–28
128. Yang J, Vais H, Gu W, Foskett JK. 2016. Biphasic regulation of $InsP_3$ receptor gating by dual Ca^{2+} release channel BH3-like domains mediates Bcl-x_L control of cell viability. *PNAS* 113:E1953–62
129. Mery L, Magnino F, Schmidt K, Krause KH, Dufour JF. 2001. Alternative splice variants of hTrp4 differentially interact with the C-terminal portion of the Inositol 1,4,5-trisphosphate receptors. *FEBS Lett.* 487:377–83
130. Fredericks GJ, Hoffmann FW, Rose AH, Osterheld HJ, Hess FM, et al. 2014. Stable expression and function of the inositol 1,4,5-triphosphate receptor requires palmitoylation by a DHHC6/selenoprotein K complex. *PNAS* 111:16478–83
131. Szado T, Vanderheyden V, Parys JB, De Smedt H, Rietdorf K, et al. 2008. Phosphorylation of inositol 1,4,5-trisphosphate receptors by protein kinase B/Akt inhibits Ca^{2+} release and apoptosis. *PNAS* 105:2427–32
132. Khan MT, Wagner L 2nd, Yule DI, Bhanumathy C, Joseph SK. 2006. Akt kinase phosphorylation of inositol 1,4,5-trisphosphate receptors. *J. Biol. Chem.* 281:3731–37
133. Hornbeck PV, Kornhauser JM, Tkachev S, Zhang B, Skrzypek E, et al. 2012. PhosphoSitePlus: a comprehensive resource for investigating the structure and function of experimentally determined post-translational modifications in man and mouse. *Nucleic Acids Res.* 40:D261–70
134. Mertins P, Yang F, Liu T, Mani DR, Petyuk VA, et al. 2014. Ischemia in tumors induces early and sustained phosphorylation changes in stress kinase pathways but does not affect global protein levels. *Mol. Cell. Proteom.* 13:1690–704
135. McEntagart M, Williamson KA, Rainger JK, Wheeler A, Seawright A, et al. 2016. A restricted repertoire of de novo mutations in *ITPR1* cause Gillespie syndrome with evidence for dominant-negative effect. *Am. J. Hum. Genet.* 98:981–92
136. Gerber S, Alzayady KJ, Burglen L, Brémond-Gignac D, Marchesin V, et al. 2016. Recessive and dominant de novo *ITPR1* mutations cause Gillespie syndrome. *Am. J. Hum. Genet.* 98:971–80
137. Ando H, Mizutani A, Kiefer H, Tsuzurugi D, Michikawa T, Mikoshiba K. 2006. IRBIT suppresses IP_3 receptor activity by competing with IP_3 for the common binding site on the IP_3 receptor. *Mol. Cell* 22:795–806
138. Kawaai K, Ando H, Satoh N, Yamada H, Ogawa N, et al. 2017. Splicing variation of Long-IRBIT determines the target selectivity of IRBIT family proteins. *PNAS* 114:3921–26
139. Bonneau B, Nougarede A, Prudent J, Popgeorgiev N, Peyrieras N, et al. 2014. The Bcl-2 homolog Nrz inhibits binding of IP_3 to its receptor to control calcium signaling during zebrafish epiboly. *Sci. Signal.* 7:ra14

140. Fos C, Becart S, Canonigo Balancio AJ, Boehning D, Altman A. 2014. Association of the EF-hand and PH domains of the guanine nucleotide exchange factor SLAT with IP_3 receptor 1 promotes Ca^{2+} signaling in T cells. *Sci. Signal.* 7:ra93
141. Tu JC, Xiao B, Yuan JP, Lanahan AA, Leoffert K, et al. 1998. Homer binds a novel proline-rich motif and links group 1 metabotropic glutamate receptors with IP_3 receptors. *Neuron* 21:717–26
142. Kang S, Kwon H, Wen H, Song Y, Frueh D, et al. 2011. Global dynamic conformational changes in the suppressor domain of IP_3 receptor by stepwise binding of the two lobes of calmodulin. *FASEB J.* 25:840–50
143. Geyer M, Huang F, Sun Y, Vogel SM, Malik AB, et al. 2015. Microtubule-associated protein EB3 regulates IP_3 receptor clustering and Ca^{2+} signaling in endothelial cells. *Cell Rep.* 12:79–89
144. Tu H, Tang TS, Wang Z, Bezprozvanny I. 2004. Association of type 1 inositol 1,4,5-trisphosphate receptor with AKAP9 (Yotiao) and protein kinase A. *J. Biol. Chem.* 279:19375–82
145. Ivanova H, Ritaine A, Wagner L, Luyten T, Shapovalov G, et al. 2016. The trans-membrane domain of Bcl-2α, but not its hydrophobic cleft, is a critical determinant for efficient IP_3 receptor inhibition. *Oncotarget* 7:55704–20
146. Yamada M, Miyawaki A, Saito K, Nakajima T, Yamamoto-Hino M, et al. 1995. The calmodulin-binding domain in the mouse type 1 inositol 1,4,5-trisphosphate receptor. *Biochem. J.* 308(Part 1):83–88
147. Hirota J, Ando H, Hamada K, Mikoshiba K. 2003. Carbonic anhydrase-related protein is a novel binding protein for inositol 1,4,5-trisphosphate receptor type 1. *Biochem. J.* 372:435–41
148. Hirota J, Furuichi T, Mikoshiba K. 1999. Inositol 1,4,5-trisphosphate receptor type 1 is a substrate for caspase-3 and is cleaved during apoptosis in a caspase-3-dependent manner. *J. Biol. Chem.* 274:34433–37
149. Kopil CM, Vais H, Cheung KH, Siebert AP, Mak DO, et al. 2011. Calpain-cleaved type 1 inositol 1,4,5-trisphosphate receptor ($InsP_3R1$) has $InsP_3$-independent gating and disrupts intracellular Ca^{2+} homeostasis. *J. Biol. Chem.* 286:35998–6010
150. Schulman JJ, Wright FA, Kaufmann T, Wojcikiewicz RJ. 2013. The Bcl-2 protein family member Bok binds to the coupling domain of inositol 1,4,5-trisphosphate receptors and protects them from proteolytic cleavage. *J. Biol. Chem.* 288:25340–49
151. Lee B, Vermassen E, Yoon SY, Vanderheyden V, Ito J, et al. 2006. Phosphorylation of IP_3R1 and the regulation of $[Ca^{2+}]_i$ responses at fertilization: a role for the MAP kinase pathway. *Development* 133:4355–65
152. Zhang N, Yoon SY, Parys JB, Fissore RA. 2015. Effect of M-phase kinase phosphorylations on type 1 inositol 1,4,5-trisphosphate receptor-mediated Ca^{2+} responses in mouse eggs. *Cell Calcium* 58:476–88
153. Cui J, Matkovich SJ, deSouza N, Li S, Rosemblit N, Marks AR. 2004. Regulation of the type 1 inositol 1,4,5-trisphosphate receptor by phosphorylation at tyrosine 353. *J. Biol. Chem.* 279:16311–16
154. Kettenbach AN, Schweppe DK, Faherty BK, Pechenick D, Pletnev AA, Gerber SA. 2011. Quantitative phosphoproteomics identifies substrates and functional modules of Aurora and Polo-like kinase activities in mitotic cells. *Sci. Signal.* 4:rs5
155. Malathi K, Kohyama S, Ho M, Soghoian D, Li X, et al. 2003. Inositol 1,4,5-trisphosphate receptor (type 1) phosphorylation and modulation by Cdc2. *J. Cell. Biochem.* 90:1186–96
156. Maxwell JT, Natesan S, Mignery GA. 2012. Modulation of inositol 1,4,5-trisphosphate receptor type 2 channel activity by Ca^{2+}/calmodulin-dependent protein kinase II (CaMKII)-mediated phosphorylation. *J. Biol. Chem.* 287:39419–28
157. Daub H, Olsen JV, Bairlein M, Gnad F, Oppermann FS, et al. 2008. Kinase-selective enrichment enables quantitative phosphoproteomics of the kinome across the cell cycle. *Mol. Cell* 31:438–48
158. Humphrey SJ, Yang G, Yang P, Fazakerley DJ, Stockli J, et al. 2013. Dynamic adipocyte phosphoproteome reveals that Akt directly regulates mTORC2. *Cell Metab.* 17:1009–20
159. Tsai CF, Wang YT, Yen HY, Tsou CC, Ku WC, et al. 2015. Large-scale determination of absolute phosphorylation stoichiometries in human cells by motif-targeting quantitative proteomics. *Nat. Commun.* 6:6622
160. Sliter DA, Aguiar M, Gygi SP, Wojcikiewicz RJ. 2011. Activated inositol 1,4,5-trisphosphate receptors are modified by homogeneous Lys-48- and Lys-63-linked ubiquitin chains, but only Lys-48-linked chains are required for degradation. *J. Biol. Chem.* 286:1074–82

161. Wagner SA, Beli P, Weinert BT, Scholz C, Kelstrup CD, et al. 2012. Proteomic analyses reveal divergent ubiquitylation site patterns in murine tissues. *Mol. Cell. Proteom.* 11:1578–85
162. Lundby A, Lage K, Weinert BT, Bekker-Jensen DB, Secher A, et al. 2012. Proteomic analysis of lysine acetylation sites in rat tissues reveals organ specificity and subcellular patterns. *Cell Rep.* 2:419–31
163. Haun S, Sun L, Hubrack S, Yule D, Machaca K. 2012. Phosphorylation of the rat Ins(1,4,5)P_3 receptor at T930 within the coupling domain decreases its affinity to Ins(1,4,5)P_3. *Channels* 6:379–84
164. Boutin B, Tajeddine N, Monaco G, Molgo J, Vertommen D, et al. 2015. Endoplasmic reticulum Ca^{2+} content decrease by PKA-dependent hyperphosphorylation of type 1 IP_3 receptor contributes to prostate cancer cell resistance to androgen deprivation. *Cell Calcium* 57:312–20
165. Gomez L, Thiebaut PA, Paillard M, Ducreux S, Abrial M, et al. 2016. The SR/ER-mitochondria calcium crosstalk is regulated by GSK3β during reperfusion injury. *Cell Death Differ.* 23:313–22
166. Barresi S, Niceta M, Alfieri P, Brankovic V, Piccini G, et al. 2017. Mutations in the IRBIT domain of *ITPR1* are a frequent cause of autosomal dominant nonprogressive congenital ataxia. *Clin. Genet.* 91:86–91
167. Ohba C, Osaka H, Iai M, Yamashita S, Suzuki Y, et al. 2013. Diagnostic utility of whole exome sequencing in patients showing cerebellar and/or vermis atrophy in childhood. *Neurogenetics* 14:225–32
168. Sasaki M, Ohba C, Iai M, Hirabayashi S, Osaka H, et al. 2015. Sporadic infantile-onset spinocerebellar ataxia caused by missense mutations of the inositol 1,4,5-triphosphate receptor type 1 gene. *J. Neurol.* 262:1278–84
169. Huang L, Chardon JW, Carter MT, Friend KL, Dudding TE, et al. 2012. Missense mutations in *ITPR1* cause autosomal dominant congenital nonprogressive spinocerebellar ataxia. *Orphanet J. Rare Dis.* 7:67
170. Hara K, Shiga A, Nozaki H, Mitsui J, Takahashi Y, et al. 2008. Total deletion and a missense mutation of *ITPR1* in Japanese SCA15 families. *Neurology* 71:547–51
171. Yamazaki H, Nozaki H, Onodera O, Michikawa T, Nishizawa M, Mikoshiba K. 2011. Functional characterization of the P1059L mutation in the inositol 1,4,5-trisphosphate receptor type 1 identified in a Japanese SCA15 family. *Biochem. Biophys. Res. Commun.* 410:754–58
172. Schnekenberg RP, Perkins EM, Miller JW, Davies WI, D'Adamo MC, et al. 2015. *De novo* point mutations in patients diagnosed with ataxic cerebral palsy. *Brain* 138:1817–32
173. Hamada K, Terauchi A, Nakamura K, Higo T, Nukina N, et al. 2014. Aberrant calcium signaling by transglutaminase-mediated posttranslational modification of inositol 1,4,5-trisphosphate receptors. *PNAS* 111:E3966–75
174. Boulay G, Brown DM, Qin N, Jiang M, Dietrich A, et al. 1999. Modulation of Ca^{2+} entry by polypeptides of the inositol 1,4,5-trisphosphate receptor (IP_3R) that bind transient receptor potential (TRP): evidence for roles of TRP and IP_3R in store depletion-activated Ca^{2+} entry. *PNAS* 96:14955–60
175. Bononi A, Giorgi C, Patergnani S, Larson D, Verbruggen K, et al. 2017. BAP1 regulates IP_3R3-mediated Ca^{2+} flux to mitochondria suppressing cell transformation. *Nature* 546:549–53
176. Kuchay S, Giorgi C, Simoneschi D, Pagan J, Missiroli S, et al. 2017. PTEN counteracts FBXL2 to promote IP_3R3- and Ca^{2+}-mediated apoptosis limiting tumour growth. *Nature* 546:554–58
177. Khan MT, Bhanumathy CD, Schug ZT, Joseph SK. 2007. Role of inositol 1,4,5-trisphosphate receptors in apoptosis in DT40 lymphocytes. *J. Biol. Chem.* 282:32983–90
178. Matsu-Ura T, Shirakawa H, Suzuki KGN, Miyamoto A, Sugiura K, et al. 2019. Dual-FRET imaging of IP_3 and Ca^{2+} revealed Ca^{2+}-induced IP_3 production maintains long lasting Ca^{2+} oscillations in fertilized mouse eggs. *Sci. Rep.* 9:4829
179. Lock JT, Alzayady KJ, Yule DI, Parker I. 2018. All three IP_3 receptor isoforms generate Ca^{2+} puffs that display similar characteristics. *Sci. Signal.* 11:eaau0344
180. Prole DL, Taylor CW. 2019. Structure and function of IP_3 receptors. *Cold Spring Harb. Perspect. Biol.* 11. **https://doi.org/10.1101/cshperspect.a035063**
181. Uhlén P, Laestadius A, Jahnukainen T, Söderblom T, Bäckhed F, et al. 2000. α-Haemolysin of uropathogenic *E. coli* induces Ca^{2+} oscillations in renal epithelial cells. *Nature* 405:694–97
182. Wang L, Wagner LE 2nd, Alzayady KJ, Yule DI. 2017. Region-specific proteolysis differentially regulates type 1 inositol 1,4,5-trisphosphate receptor activity. *J. Biol. Chem.* 292:11714–26

183. Miyamoto A, Miyauchi H, Kogure T, Miyawaki A, Michikawa T, Mikoshiba K. 2015. Apoptosis induction-related cytosolic calcium responses revealed by the dual FRET imaging of calcium signals and caspase-3 activation in a single cell. *Biochem. Biophys. Res. Commun.* 460:82–87
184. Mikoshiba K, Okano H, Tsukada Y. 1985. P_{400} protein characteristic to Purkinje cells and related proteins in cerebella from neuropathological mutant mice: autoradiographic study by ^{14}C-leucine and phosphorylation. *Dev. Neurosci.* 7:179–87
185. Pober JS, Sessa WC. 2007. Evolving functions of endothelial cells in inflammation. *Nat. Rev. Immunol.* 7:803–15
186. Minichiello L. 2009. TrkB signalling pathways in LTP and learning. *Nat. Rev. Neurosci.* 10:850–60
187. De Bock M, Wang N, Decrock E, Bol M, Gadicherla AK, et al. 2013. Endothelial calcium dynamics, connexin channels and blood-brain barrier function. *Prog. Neurobiol.* 108:1–20
188. Feske S, Skolnik EY, Prakriya M. 2012. Ion channels and transporters in lymphocyte function and immunity. *Nat. Rev. Immunol.* 12:532–47